https://doi.org/10.5194/egusphere-2026-2458
Preprint. Discussion started: 30 April 2026

Ice nucleating properties of α-pinene- and limonene-derived secondary organic aerosol under cirrus conditions

Christopher N. Rapp[1], Sining Niu[2], Jason D. Surratt[3,4], Yue Zhang[2], Daniel J. Cziczo[1]

[1]Department of Earth, Atmospheric and Planetary Sciences, Purdue University, West Lafayette, Indiana, 47906-2051, USA
[2]Department of Atmospheric Sciences, Texas A&M University, College Station, Texas, 77843-3150, USA
[3]Department of Environmental Sciences and Engineering, University of North Carolina at Chapel Hill, Chapel Hill, North Carolina, 27599-7400, USA
[4]Department of Chemistry, University of North Carolina at Chapel Hill, Chapel Hill, North Carolina, 27599-3290, USA

Correspondence to: Daniel J. Cziczo (djcziczo@purdue.edu)

Abstract

The contribution of biogenic secondary organic aerosol (BSOA) to cirrus cloud formation remains unresolved, contributing to uncertainty in aerosol-cloud interactions in global climate models. Laboratory studies report highly variable ice nucleating efficiencies for BSOA, suggesting that these particles may act as either homogeneous or moderately effective heterogeneous ice nuclei. Here, we investigate the deposition ice nucleating properties of α-pinene- and limonene-derived BSOA, including both self-nucleated particles and BSOA coatings on ammonium sulfate and ammonium bisulfate seed particles. Deposition ice nucleation relevant to cirrus clouds (−45°C, −40°C, −35°C; $1.0 \leq S_{ice} \leq 1.6$) was measured using the SPectrometer for Ice Nucleation (SPIN). Bulk physicochemical properties relevant to ice nucleation were characterized using aerosol mass spectrometry (AMS) and volatility distributions. Pre-cooling was applied to modulate phase state as inferred from glass transition temperature (T_g).

BSOA ice nucleating properties were strongly precursor dependent ($p < 0.001$). T_g was an unreliable predictor of freezing behavior, correctly anticipating freezing mode for only two of eleven particle combinations. Limonene-derived BSOA nucleated ice almost exclusively via heterogeneous freezing, with S_{ice} onsets as low as 1.27±0.07 at -39.8±0.3°C. α-pinene-derived BSOA predominantly nucleated ice homogeneously. BSOA coatings on ammonium bisulfate shifted freezing from homogeneous to heterogeneous, while the role of acid-catalyzed multiphase chemistry in ice nucleation remained inconclusive due to experimental limitations. These results demonstrate that cirrus-relevant BSOA parameterizations must explicitly account for precursor specific chemistry and broad classifications of BSOA ice nucleating abilities are inappropriate.

1 Introduction

Cirrus are upper tropospheric clouds composed entirely of ice and exhibit extensive global coverage, particularly in the tropical latitudes (Heymsfield et al., 2017). They exert a significant influence on Earth's climate and weather by scattering incoming solar radiation and absorbing outgoing infrared radiation. Recent global assessments indicate that cirrus contribute to both positive (warming, high confidence) and negative (cooling, low confidence) climate feedbacks (Boucher et al., 2013; Forster et al., 2021). These feedbacks depend on general cloud properties such as altitude, coverage, and cloud opacity (Zelinka et al., 2017), as well as microphysical characteristics including ice crystal number concentration and size (Lohmann et al., 2008). Atmospheric aerosol strongly affect cloud properties (Albrecht, 1989; Twomey et al., 1984), with the uncertainty in effective radiative forcing due to these aerosol-cloud interactions remaining larger than that associated with any other identified climate forcing from other atmospheric trace constituents (Forster et al., 2021). This limitation is particularly acute for ice-containing clouds such as cirrus, for which global climate model representation is "considerably less advanced than that involving liquid-only clouds" (Boucher et al., 2013).

https://doi.org/10.5194/egusphere-2026-2458
Preprint. Discussion started: 30 April 2026

Ice crystals in cirrus form through two primary pathways: homogeneous or heterogenous freezing. Homogeneous freezing occurs at temperatures below approximately -38°C and under highly supersaturated conditions with respect to ice ($S_{ice} \gtrsim 1.5$) where solution droplets freeze spontaneously (Koop et al., 2000; Pruppacher and Klett, 2010). In contrast, heterogeneous freezing is initiated by ice nucleating particles (INPs), a small subset of atmospheric aerosol particles which catalyze ice formation at warmer temperatures and lower supersaturations (Pruppacher and Klett, 2010). There is compelling evidence a majority of cirrus formation is initiated by heterogeneous nucleation (Cziczo et al., 2013); however, competition between the two processes (Kärcher et al., 2022) is dependent on the underlying atmospheric dynamics that dictate available water vapor and temperature (Heymsfield et al., 2017).

Several heterogeneous freezing modes are relevant to cirrus formation (Heymsfield et al., 2017). In immersion freezing, an INP is engulfed in liquid water that subsequently freezes upon sufficient cooling (Heymsfield et al., 2017; Pruppacher and Klett, 2010). Deposition nucleation, in the classical sense, involves the direct transition of water vapor to ice on an INP under ice supersaturated conditions without an intervening liquid phase (Pruppacher and Klett, 2010). Freezing below water saturation has also been explained by pore condensation and freezing (PCF), in which liquid first condenses within surface imperfections or cavities (i.e. pores) due to the inverse Kelvin effect before freezing and subsequent ice growth (Marcolli, 2014). Observational and modeling studies suggest cirrus formation predominantly occurs via deposition nucleation (Cziczo et al., 2013; Hendricks et al., 2011).

The composition of INPs relevant to cirrus clouds are highly variable. Laboratory studies demonstrate that mineral dust, anhydrous salts, organics, black carbon, and biological particles exhibit a wide range of ice nucleating efficiencies (Hoose and Möhler, 2012). Among these types, organic particles arguably remain the least understood (Knopf et al., 2018), despite constituting a substantial fraction of tropospheric aerosol mass (Hallquist et al., 2009; Shrivastava et al., 2017). Aircraft measurements indicate that cirrus ice residuals (IRs), particles remaining after evaporating ice from hydrometeors, are predominantly mineral dust for both convective outflow (anvil) and synoptically formed cirrus (Cziczo et al., 2017; Cziczo and Froyd, 2014), with organic-sulfate containing IRs accounting for only 14% (Cziczo et al., 2013). In contrast, subvisible cirrus IRs in the tropical upper troposphere are dominated (~ 96%, +/- ion modes) by organic-sulfate containing species with sulfate existing in both neutralized and acidic forms (Froyd et al., 2010). Ground-based ice nucleation measurements further identify ambient organic species as a source of cirrus INPs, albeit with low activation fractions (Wolf et al., 2020). Collectively, these observations underscore the relevance of organic aerosol in cirrus formation.

Organic particles are challenging to characterize because their aerosol phase state strongly influences their ice nucleating ability. They can exist in liquid, amorphous semi-solid, or amorphous solid ("glassy") states (Koop et al., 2011), with the latter two high viscosity phase states being identified as a requirement for heterogeneous freezing to occur (Knopf et al., 2018; Li et al., 2024; Murray et al., 2010). Some organics can also be crystalline (Mahrt et al., 2025) but for the purposes of this article the focus will be on amorphous non-crystalline organics. Global modeling studies indicate that most organic particles at cirrus cloud altitudes are expected to be glassy (Shiraiwa et al., 2017), with temperature and relative humidity (RH) as key modulators of phase state (Koop et al., 2011).

Directly measuring particle viscosity to determine phase state is not always feasible (Grayson et al., 2017), so the transition between an amorphous semi-solid to an amorphous solid-like glass state is frequently parameterized by the glass transition temperature, T_g (Koop et al., 2011). Unlike first-order transitions (i.e., melting or boiling) with an exact temperature, T_g is a "non-equilibrium transition that occurs over a temperature interval" and is sensitive to kinetic factors such as cooling or drying rates (Koop et al., 2011). In the presence of water vapor (i.e., high RH), T_g will be depressed since water will dilute the organic mass fraction of the particle, effectively acting as a plasticizer. This RH dependence can be accounted for using a binary organic-water form of the Gordon-Taylor equation (Koop et al., 2011) and represented as a function of the organic mass fraction, $T_g(\omega_{org})$. While a semi-solid or glassy phase state may be necessary for heterogeneous freezing, experimental studies indicate that a glassy phase alone does not guarantee ice nucleation (Kasparoglu et al., 2022; Rapp et al., 2025b).

https://doi.org/10.5194/egusphere-2026-2458
Preprint. Discussion started: 30 April 2026

For this study, we focus on secondary organic aerosol (SOA) derived from biogenic sources (BSOA). BSOA forms when biogenic volatile organic compounds (BVOCs) emitted from the biosphere are oxidized by reactive species such as ozone (O_3), hydroxyl radicals ($^{\bullet}OH$) or nitrate radicals ($NO_3^{\bullet}$). The resulting low-volatility products then undergo gas-particle partitioning via new particle formation, condensation onto pre-existing aerosol, or multiphase reactions (Nozière et al., 2015). Annual BSOA production is estimated to be between 22 and 24 Tg globally (Pye et al., 2010). BVOC emissions are dominated by isoprene and followed by emissions of as α-pinene, t-β-ocimene, β-pinene, and limonene (Guenther et al., 2012). We note that estimates of BSOA production and BVOC emissions vary across studies and are frequently reevaluated as new measurements are obtained or models are refined. As such, we refer the reader to the following reviews and the references therein (Hallquist et al., 2009; Shrivastava et al., 2017).

Laboratory studies of BSOA ice nucleation in the cirrus regime have primarily examined particles formed via self-nucleation and/or condensation onto pre-existing seed particles (Charnawskas et al., 2017; Ignatius et al., 2016; Kasparoglu et al., 2022; Koehler et al., 2010; Kulkarni et al., 2016; Ladino et al., 2014; Möhler et al., 2008; Piedehierro et al., 2021; Wagner et al., 2017). α-Pinene is the most studied BSOA precursor followed by limonene. A consensus among these studies is self-nucleated α-pinene and limonene BSOA contribute to cirrus formation predominantly by homogeneous freezing, with exceptions being due to some form of particle preconditioning. First, self-nucleated α-pinene BSOA pre-cooled to -40°C exhibited heterogeneous freezing at lower ice saturations S_{ice}, suggesting either a highly viscous phase state was obtained or pre-activation occurred (Ladino et al., 2014). Convective ice-cloud processing of α-pinene BSOA in the Aerosol Interaction and Dynamics in the Atmosphere (AIDA) chamber produced highly porous particles that froze heterogeneously (Wagner et al., 2017). Highly viscous α-pinene BSOA generated in a cold low humidity cloud chamber (RH_w < 15%, -38°C < T < -10°C) have also nucleated ice heterogeneously at significantly warmer temperatures than other studies (Ignatius et al., 2016). In contrast, the use of extremely dry and pre-cooled (-25°C) glassy BSOA only froze homogeneously under free tropospheric conditions (Kasparoglu et al., 2022).

Coatings of organic material on seed particles generally suppress or deactivate INPs. For example, fully coated mineral dust or soot exhibit reduced nucleation efficiency compared with bare seeds or partially coated particles (Koehler et al., 2010; Kulkarni et al., 2016; Möhler et al., 2008). Similarly, α-pinene BSOA-coated ammonium sulfate particles preconditioned to low RH nucleated ice homogeneously (Piedehierro et al., 2021). In contrast, deposition ice nucleation of α-pinene BSOA coated soot has been observed for temperatures less than -53°C and was irrespective of coating thickness, but atomic O:C ratio showed an effect by modulating phase state (Charnawskas et al., 2017).

Ice nucleation studies of BSOA formed through multiphase reactions remain limited despite their global importance. Low-volatility oxygenated organosulfates (OS), produced via oxidation of BVOCs in the presence of acidified sulfate seed aerosol have been observed to contribute significantly to total organic aerosol mass, with estimates ranging from 5 to 30% and that isoprene-derived OS substantially contribute to this mass fraction (Brüggemann et al., 2020; Glasius et al., 2018; Hettiyadura et al., 2019; Surratt et al., 2008). Sulfate seed acidity has also shown to strongly influence aerosol phase state for SOA formed by the reactive uptake of isoprene-derived epoxydiols (IEPOX) (Lei et al., 2022) and by extension heterogeneous freezing potential. Ambient ground-based measurements have identified IEPOX-derived organosulfate ion markers in ice residuals and filter samples, indicating they may be an important source of BSOA INPs (Wolf et al., 2020). Laboratory studies of synthesized constituents of IEPOX-derived SOA have also been determined to be INP (Wolf et al., 2020), but strongly depend on phase state (Li et al., 2024). Collectively, these findings underscore the need for systematic investigation of BSOA generated via acid-catalyzed multiphase reactions on sulfate aerosols as cirrus INPs, especially from terpenes that are larger than isoprene such as α-pinene and limonene.

To address critical uncertainties surrounding the role of BSOA in cirrus cloud formation and their implications for Earth's climate, we experimentally investigated the deposition ice nucleating properties of self-nucleated α-pinene- and limonene-derived BSOA, as well as their coatings on ammonium sulfate (AS) and partially neutralized sulfate (PNS) particles, under cirrus conditions. Coating thickness was verified by measuring the increase in particle diameter for size-selected seed particles. Particle composition, volatility, and T_g were characterized to constrain aerosol physicochemical properties and infer phase state. The influence of phase state on ice nucleation was evaluated through controlled pre-cooling experiments, while chemical

https://doi.org/10.5194/egusphere-2026-2458
Preprint. Discussion started: 30 April 2026

ionization mass spectrometry was used to identify the formation of OS associated with acid-catalyzed multiphase chemistry. Using these systematic measurements, we tested the following hypotheses:

- **H1**: Self-nucleated α-pinene- and limonene-derived BSOA can only nucleate ice homogeneously - *rejected*.
- **H2**: The ice nucleating properties of BSOA are independent of precursor identity - *rejected*.
- **H3**: BSOA warmer than their respective T_g will only nucleate ice homogeneously - *rejected*.
- **H4**: Multiphase chemistry does not influence the ice nucleating properties of α-pinene and limonene BSOA-coated sulfate particles - *inconclusive*.

2 Methods

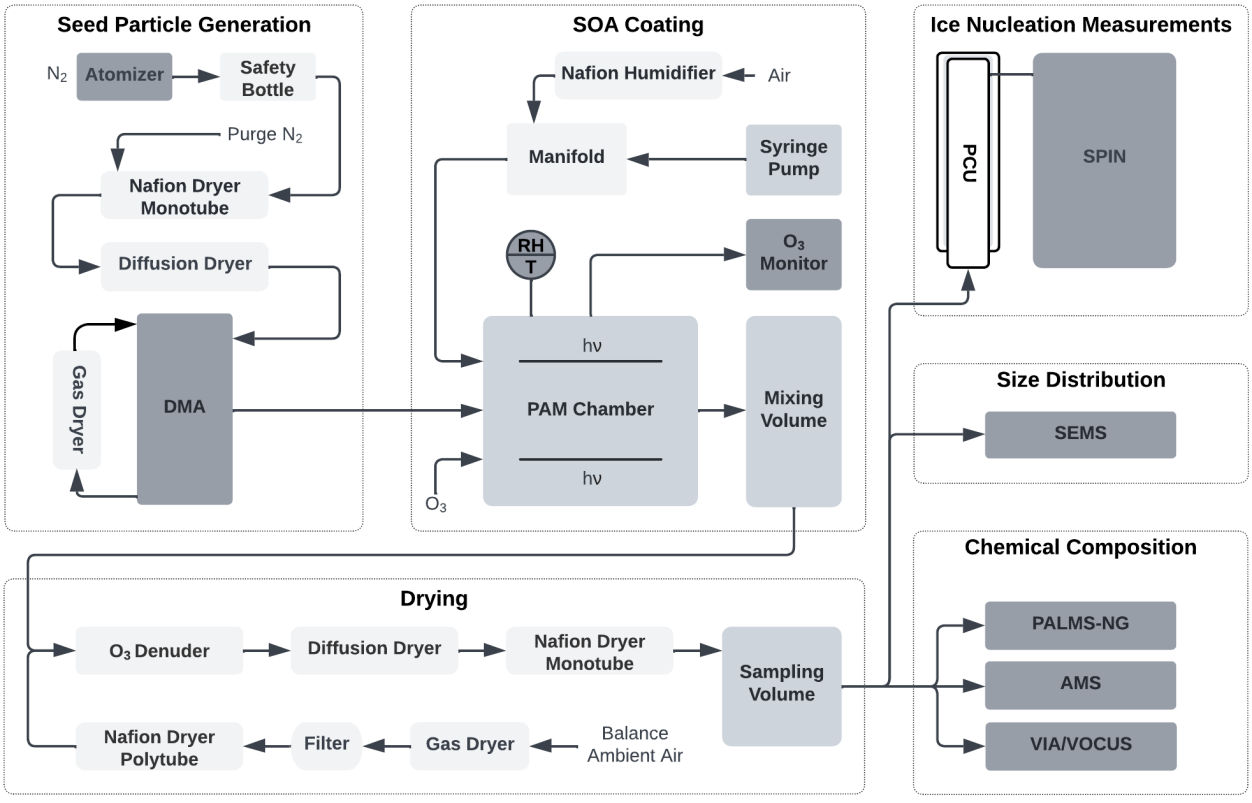

Figure 1 – Experimental setup for sulfate salt SOA coating experiments summarizing the following stages: seed particle generation, SOA coating, drying, chemical composition measurements, size distribution measurements, pre-cooling, and ice nucleation measurement. For self-nucleated SOA experiments, ultra-high purity nitrogen gas was sent through the PAM oxidation flow reactor instead of sulfate seed particles. Detailed steps corresponding to each experimental stage can be found in the methods.

2.1 Materials

Sulfate seed particles were generated from 0.025 M and 0.02 M solutions of ammonium sulfate (AS, $(NH_4)_2SO_4$, ≥ 99 %, A4915; Sigma-Aldrich) and ammonium bisulfate (ABS, NH_4HSO_4, ≥ 99.99 %, 455849; Sigma-Aldrich), respectively. Commercial monoterpenes (-)-α-pinene (α-pinene, ≥ 99 %, 274399; Sigma-Aldrich) and (R)-(+)-limonene (limonene, ≥ 97 %, 183164; Sigma-Aldrich) were selected as chemical precursors for SOA.

https://doi.org/10.5194/egusphere-2026-2458
Preprint. Discussion started: 30 April 2026

We note that ABS seed particles were produced directly from ABS salt rather than from an equimolar mixture of AS and sulfuric acid (H_2SO_4). This approach was chosen to provide an unambiguous reference for homogeneous freezing (see Sect. 2.6.2 and 3.1.1); however, it is known to also affect acid-catalyzed chemistry (Sect. 4.1). In addition, partial neutralization of ABS-derived seed particles was observed during repeated SOA coating experiments conducted after all ice nucleation experiments (Sect. 3.3). As a result, we cannot definitively be classified as ABS, although "fresh" ABS experiments exhibited homogeneous freezing as expected. Hereafter, references to particles generated from ABS salt are referred to as partially neutralized sulfate (PNS).

2.2 Aerosol generation

2.2.1 Seed particle generation

Aerosol was generated by atomizing (Model 3076; TSI Inc., Shoreview, MN 3077) solutions of ammoniated sulfate at a flow rate of 0.9 L min^{-1} using compressed ultra-high purity nitrogen gas (UHP N_2, Indiana Oxygen, Lafayette, IN). An Erlenmeyer flask followed the atomizer to collect any condensation and prevent liquid from collecting in aerosol sampling lines. Aerosol were dried (RH < 20%) below the efflorescence RH of AS (33±2%) particles to induce crystallization (Cziczo et al., 1997). Given the ABS salt was partially neutralized, the resultant PNS particles could have also crystallized (i.e., letovicite). Drying was performed using a 30.5-cm Nafion™ dryer (Model MD-700-12S-3; Perma Pure LLC, Lakewood, NJ) operating at purge UHP N_2 to sample flow ratio of 3:1 followed by a 43-cm desiccant diffusion dryer. Particles were charge neutralized (Aerosol Charge Neutralizer, Model 9000; Brechtel Manufacturing Inc., Hayward, CA) and size selected with an electrical mobility diameter of 300 nm using a differential mobility analyzer (DMA, Model 3081A; TSI Inc., Shoreview, MN) installed in an electrostatic classifier (Model 3082; TSI Inc., Shoreview, MN) and operated at a 10:1 sheath-to-sample flow ratio. To maintain RH < 10% in the DMA, an in-line desiccant gas dryer was used to dry the sheath flow. A full schematic of aerosol generation can be found in Fig. 1.

2.2.2 Precursor oxidation

BSOA-coated and self-nucleated aerosol were generated using the Potential Aerosol Mass oxidation flow reactor (PAM-OFR, Aerodyne Research Inc., Billerica, MA) which is described in detailed elsewhere (Lambe et al., 2011b). The configuration used for this study was a 13.3 L glass cylinder with four internal ultraviolet (UV) mercury lamps (254 nm) to photolyze ozone (O_3) in the presence of water vapor and produce hydroxyl radicals ($^{\bullet}OH$). For coating experiments, 0.9 L min^{-1} of particle-laden air was introduced into the chamber, while filtered compressed air was used for self-nucleation experiments. O_3 was continuously introduced into the PAM-OFR by passing 0.3 L min^{-1} of compressed air (THC < 1 ppm, Indiana Oxygen, Lafayette, IN) through an enclosed vessel containing a mercury UV lamp producing 185 nm light (95-2100-3; Jelight Company Inc., Irvine, CA). Both O_3 concentration and UV intensity were controlled using custom-built constant output voltage regulators. Liquid VOC precursors were continuously injected into a triple-necked round bottom flask using a syringe pump (Fusion 100T; Chemyx, Stafford, TX) with gas-phase precursor concentration controlled by injection rate (see Table 1 for summary). Compressed air was humidified using a Nafion™ flowtube (Model PD-50T-12MSS; Perma Pure LLC, Lakewood, NJ) coupled with a frit bubbler filled with deionized water and carried the volatilized precursors into the PAM-OFR at a flow rate of 0.3 L min^{-1}. PAM-OFR temperature and humidity was continuously measured using a hygro-thermistor (UX100-023A; HOBO, Bourne, MA) and O_3 concentration measured with an O_3 monitor (Model 106-L, 2B Technologies, Broomfield, CO) with a flow rate of 0.6 - 0.8 L min^{-1}.

Following the PAM-OFR, a 10 L mixing volume was positioned to increase reaction time (total reaction time of ~ 20 to 23 mins) and promote heterogeneous (multiphase) reactions of VOC oxidation products with sulfate seed aerosols. Aerosol were then sequentially sampled through a denuder to remove O_3, a 43-cm desiccant diffusion dryer, and a Nafion™ dryer (Model MD-700-12S-3; Perma Pure LLC, Lakewood, NJ) operating at 3:1 UHP N_2 purge to sample ratio. As the exiting flow rate of the PAM-OFR was 0.7 - 0.9 L min^{-1}, dry balance air was necessary to supply enough flow for all connected instruments downstream. This was provided using a desiccant gas dryer and Nafion™ dryer (Model PD-50T-12MSS; Perma Pure LLC, Lakewood, NJ) using the same 3:1 purge to sample flow ratio as previous dryers (see Fig. 1).

https://doi.org/10.5194/egusphere-2026-2458
Preprint. Discussion started: 30 April 2026

For each PAM-OFR experiment, the O_3 concentration and UV-C light intensity were optimized to minimize self-nucleation while maximizing SOA coating, achieving a minimum coating thickness of 10 nm (Table 1). The •OH exposure, defined as the product of the •OH concentration and the residence time in the PAM, was calculated using the time-step PAM_Chem model (Lambe et al., 2011a) with inputs including UV-C photon flux, O_3 concentration, and water vapor mixing ratio under experimental conditions. The resulting •OH exposure was converted to an equivalent atmospheric aging time using a representative 12-hour daytime global mean •OH concentration of 1.5×10^6 molecules cm^{-3} (Albaladejo et al., 2003; Lelieveld et al., 2016). This value was applied solely for post hoc reporting and was not prescribed a priori in the experimental design.

Table 1 – Conditions used in generating SOA using the PAM-OFR.

Seed Particle	Gas-phase precursor	VOC Concentration (ppb)	O_3 (ppb)	Photon flux	OH exposure (s cm^{-3})	Equivalent atmospheric aging (days)
PNS	α-pinene	170	11550	5.47×10^{13}	4.5×10^{11}	3.5
PNS	limonene	285	375	8.83×10^{13}	1.6×10^{11}	1.3
AS	α-pinene	180	11550	5.47×10^{13}	4.5×10^{11}	3.5
AS	limonene	295	375	8.83×10^{13}	1.6×10^{11}	1.3
-	α-pinene	180	11550	5.47×10^{13}	4.5×10^{11}	3.5
-	limonene	295	375	8.83×10^{13}	1.6×10^{11}	1.3

https://doi.org/10.5194/egusphere-2026-2458
Preprint. Discussion started: 30 April 2026

2.3 Multi-lognormal particle size distributions

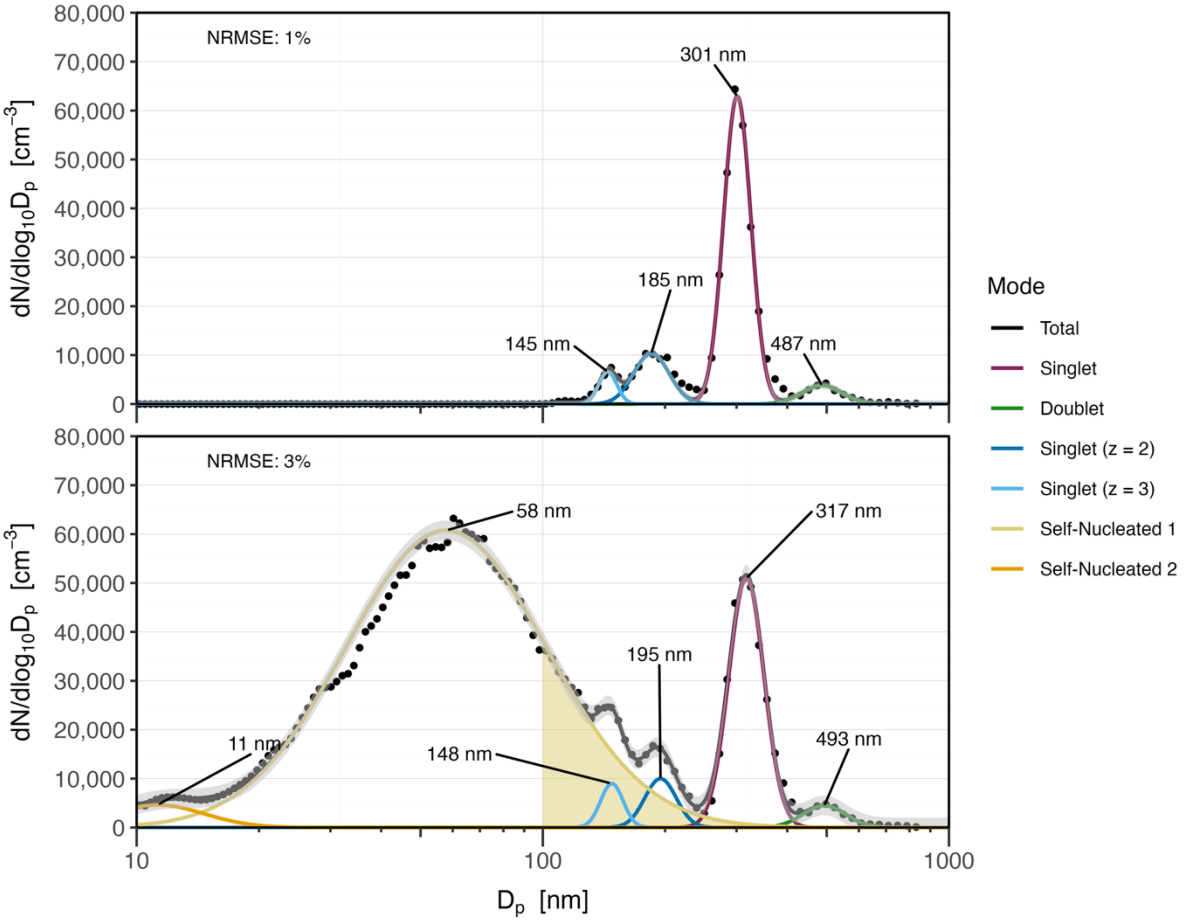

Figure 2 – Evolution of a typical PSD before and after SOA coating: (top) 300 nm size-selected PNS aerosol free of any organics and (bottom) α-pinene-PNS BSOA with two self-nucleation modes. Labels indicate the $\overline{D}_{pg}$ of the fitted mode. Gray shaded ribbon around the mode summed PSD (black) is the root mean square error interval of the total lognormal fit vs. the measured PSD. Yellow shaded region is the integrated area of particles originating from self-nucleation larger than 100 nm and relevant to ice nucleation in SPIN.

Particle size distributions (PSDs) were continuously measured using a scanning electrical mobility sizer (SEMS, Model 2002; Brechtel Manufacturing Inc., Hayward, CA). The measurement interval was modified according to the following scheme: zero count or self-nucleation testing (30 s), coating-free monodisperse sulfate seed sampling (60 s), and coating evaluation (120 s). All measurements operated at a minimum sheath-to-sample flow ratio of 10:1 with a sample flow rate of 0.25–0.3 L min^{-1}. Sheath flow RH was maintained at or below 5% for all experiments using a sheath desiccant gas dryer. PSDs frequently consisted of multiple modes corresponding to the following features: singlet, multi-charged singlets, singly charged aggregates (i.e., doublets or triplets), and/or self-nucleated SOA. To account for each particle type, a multimodal curve fitting algorithm was applied (Rapp et al., 2025a) to retrieve mode specific lognormal fitting parameters. A specific example of this algorithm applied to this study is given by Fig. 2 where modes are labeled and concentrations of self-nucleated particles relevant to ice nucleation integrated. Briefly, this algorithm iteratively subtracts lognormal PSDs from the measured distribution until convergence or maximum number of modes is met. For this study, we utilized 5-minute averages of measured PSDs with

https://doi.org/10.5194/egusphere-2026-2458
Preprint. Discussion started: 30 April 2026

algorithm parameters set to allow a maximum of eight modes and a convergence threshold of 5% max-min normalized root-square mean error in concentration and 95% of all variance in particle concentration is explained. The output of the algorithm was used to calculate the percentage of particles corresponding to either coated-sulfate seed particles or "pure" SOA (those formed by self-nucleation i.e. mode $\overline{D}_{pg} \leq 100$ nm). Furthermore, the multimodal algorithm was used to extract the following information from the particle size distribution measurements ($D_p \geq 100$ nm): percentage of self-nucleated particles, singlet to doublet concentration percentage, and singlet mode parameters ($\overline{D}_{pg}$ and σ_g). Errors for percentages were defined as the sum of fractional uncertainties based on each mode's concentration RMSE.

2.4 Chemical composition

2.4.1 PALMS-NG

Compositional measurements of the SOA-coated sulfate particles were obtained using the Particle Analysis by Laser Mass Spectrometry – Next Generation (PALMS-NG) instrument (Jacquot et al., 2024). These measurements were primarily motivated by identifying sulfate-seed ion fragments and supporting precursor identification in future aircraft studies. Spectra were collected under the same generating conditions as the ice nucleation experiments, though asynchronously to ice nucleation measurements. PALMS-NG is a single-particle mass spectrometer that samples particles at 0.5 L min^{-1} into an aerodynamic inlet, focusing them into a particle beam with minimal loss of volatile species (Murphy, 2007). Particle aerodynamic diameters are determined from size-dependent transit times between two 405 nm lasers (Jacquot et al., 2024). Detection by the second "triggering" laser prompts a 193 nm excimer laser pulse that ionizes the particle, with both positive and negative ions analyzed simultaneously by two sToF mass spectrometers (Jacquot et al., 2024). While the excimer laser ionizes nearly all atmospheric species it is quantitively limited due to matrix effects, recombination reactions, and material dependent ionization efficiencies. These limitations were minimized in this study by collecting and averaging more than 300 single particle measurements to obtain representative spectra (i.e., "fingerprints") for each SOA system.

2.4.2 AMS

A high-resolution time-of-flight AMS (HR-ToF-AMS, herein referred to as AMS) was used to quantify the bulk chemical composition of the BSOA-coated sulfate particles, and the detailed working principle has been discussed in previous studies (DeCarlo et al., 2006). Briefly, the aerosol particles were sampled at a flow rate of 0.1 L min^{-1} and then focused with an aerodynamic lens. Once the particles enter the vacuum as a narrow beam, they were directed to a vaporizer, which can flash evaporate the non-refractory aerosol particles efficiently. The evaporated compounds are then ionized with an electron impact (EI) ionizer, and the ionized molecules enter a ToF mass spectrometer for characterization. The high mass resolving power (up to 4000 FWHM) allowed sub-nominal separation of chemical formulae, providing improved constraints on the bulk composition and oxidation state of the generated SOA.

2.5 VIA-Vocus-CIMS measurements and volatility/T_g estimation

To estimate volatility distribution of the generated aerosol, the Vaporization Inlet for Aerosols (VIA) was coupled with Vocus chemical ionization mass spectrometry (VIA-Vocus-CIMS, Aerodyne, Inc.) operated in NH_4^+ reagent ion mode (Niu et al., 2025). In this setting, thermally desorbed organic vapors from particles phase were detected primarily as ammonium-adduct ions, enabling organic compounds that evaporated at different temperatures to be detected as thermograms. The volatility of organic compounds comprising the bulk SOA were estimated from their thermal desorption temperatures using the methodology established in a previous study (Niu et al., 2025). It has been shown that both the vapor pressure and viscosity were influenced by the van der Waals forces between the molecules (Thomas et al., 1979). The resulting volatility information was used to estimate the $T_{g,org}$ for each precursor-seed combination (see Table 2). Based on historical measurement data, $T_{g,org}$ can be parametrized based on volatility (C*) with a semiempirical relation as described in previous study (Li et al., 2020). Parameterized $T_{g,org}$ estimates using O:C measurements were obtained using the methods described by (DeRieux et al., 2018), with uncertainty reported as an upper bound of 21°C. Furthermore, hygroscopicity estimates from O:C AMS measurements

https://doi.org/10.5194/egusphere-2026-2458
Preprint. Discussion started: 30 April 2026

($\kappa_{O:C}$) were obtained using existing methods (Lambe et al., 2011b). Both parametrized $T_{g,org}$ and $\kappa_{O:C}$ values are shown in Table 2.

2.6 Ice nucleation measurements

2.6.1 Pre-Cooling Unit (PCU)

Aerosol were cooled to −30±1°C prior to ice nucleation measurements in the SPIN using a custom-built PCU to induce a semi-solid or glassy phase state (Rapp et al., 2025b). −30±1°C was selected based on the $T_{g,org}$ values for self-nucleated dark ozonolysis products of α-pinene and limonene (Kasparoglu et al., 2022). Briefly, the PCU is a vacuum-jacketed flow tube cooled by a recirculating chiller. Temperature and RH measurements are obtained from both the chamber midpoint and PCU inlet. A detailed description of the PCU is given by (Rapp et al., 2025b). Ice nucleation measurements were conducted for both assumed "liquid" (room-temperature experiments) and "glassy" (pre-cooled to −30±1°C) phase states for all experiments containing SOA.

2.6.2 SPectrometer for Ice Nucleation (SPIN)

Ice nucleating properties of BSOA-coated seed aerosol, self-nucleated SOA, and seed aerosol were measured using the SPIN (SPIN001, Droplet Measurement Technologies, Longmont, CO) described in detail by Garimella et al. (2016). SPIN is a continuous-flow diffusion chamber (CFDC) in an upright parallel plate configuration and consists of two plates 1.0 cm apart. During operation each plate is coated by about ~ 1 mm of ice and temperature controlled by independent refrigeration loops. To simulate cloud conditions each plate temperature is modified so that an ice saturation and temperature gradient is formed. Aerosols were sampled through a knife-edge inlet and constrained to a central lamina sheet by two sheath flows operating at a ~ 10:1 standard L min^{-1} sheath-to-sample flow ratio. Given the assumption of laminar flow, the aerosol intersect a known thermodynamic profile between the plates (Garimella et al., 2016) and the cloud conditions the aerosol particles experience was interpolated. Particles then exit the chamber and enter an isothermal segment where any particles that were activated as droplets are evaporated via the Bergeron–Wegener-Findeisen process (Pruppacher and Klett, 2010). After the evaporation segment, the particle number concentration, optical size, and scattering profile was determined on a particle-by-particle basis by an optical particle counter (OPC), with specific geometry and design described in detail elsewhere (Garimella et al., 2016). For instances where droplets exceed the capacities of the evaporation segment (termed droplet breakthrough), the scattering profile obtained by the OPC can distinguish between similarly sized ice and droplets.

The SPIN was operated to observe depositional ice nucleation or homogeneous freezing of solution droplets relevant to cirrus cloud conditions (−45, −40, −35°C; $1.0 \leq S_{ice} \leq 1.6$). Lamina temperatures were kept isothermal and S_{ice} was increased from ice saturation to 1.6 at a saturation rate of 0.015 min^{-1} for −45°C and 0.024 min^{-1} for −40 and −35°C; then decreased at the same rate to water saturation. Particle classification from the OPC was determined using the depolarization based supervised machine-learning (ML) classification method described by Rapp et al., (2025b). To account for different aerosol types and particle sizes, adjustments were made to classification parameters (see Table S1 of the supplement) and particles classified by ML as droplets below water saturation were reclassified as water uptake.

Uncertainties in CFDC measurements are primarily due to non-ideal lamina behavior or inhomogeneities in temperature control. In CFDC style instruments, particles inadvertently exit the lamina and experience lower ice saturations ("lamina-spreading"). This will inhibit or require higher than expected ice saturations to observe homogeneous freezing of a given calibration particle entering the instrument (i.e., ABS). This has led to the development of a calibration factor (DeMott et al., 2015) or correction factor (Garimella et al., 2016) to account for lower than expected particle concentrations. For the SPIN, it was determined this multiplicative correction factor (CF) ranges from 1.4 to 9.5 (Garimella et al., 2017). For the purposes of this study, a CF of 1.4 was selected as a conservative estimate of ice undercounting. In contrast to lamina spreading, inhomogeneities in temperature control has been observed to homogeneously nucleate ice from solution droplets (Koop, 2004) earlier than expected. As SPIN uses refrigerant valves to control cooling, these locations are colder than neighboring regions of the plate. Calibration measurements using monodisperse ammonium nitrate (NH_4NO_3), a homogeneous freezing calibration

https://doi.org/10.5194/egusphere-2026-2458
Preprint. Discussion started: 30 April 2026

standard, have determined that these cold spots initiate freezing within the chamber. As such, average cold plate temperatures used in interpolating temperature and ice saturation are the average of thermocouple measurements at these locations.

2.6.3 Onset quantification

Particles classified as ice and having a diameter equal to or larger than 2.5 µm were totaled for each second of data. To account for background frost, an inlet filter was used to measure particle-free periods periodically during the experiment and then subtracted from this total. Both the background frost and determined ice were corrected for lamina spreading. This total ice concentration was then divided by the total number concentration of particles larger than 100 nm (Vali, 1966) entering the SPIN to determine the activation fraction (AF). As the refrigeration valves operate in an oscillatory manner and drive freezing, AF was smoothed using a rolling median (11 s). The onset of ice nucleation (i.e., combination of temperature and S_{ice}) was defined using the following metrics: (1) fraction of particles activated as ice meets or exceeds 0.5%, (2) at least 10 datapoints consecutively meet or exceed this threshold, and (3) at least 100 observations in total must be observed. The first observation at which all metrics are satisfied is the onset temperature and S_{ice}. To be comparative to other literature, we selected the 0.5% threshold to match most recent studies investigating the ice nucleating properties of SOA or their proxies (Kasparoglu et al., 2022; Rapp et al., 2025b). For context, this value falls within activation thresholds used to classify the onset of ice nucleation for α-pinene-derived BSOA particles: 0.1% (Ladino et al., 2014; Wagner et al., 2017), 1% (Möhler et al., 2008; Piedehierro et al., 2021), and 10% (Ignatius et al., 2016). Conditions 1 and 2 to quantify onset are conservative measures to prevent reporting bursts of background frost as heterogeneous ice nuclei. Additionally, we classify a freezing onset as heterogeneous by being below the lower uncertainty range in water activity (Δa_w = -2.5%) for homogeneous freezing of 100 nm aqueous droplets (Koop, 2004; Koop et al., 2000).

https://doi.org/10.5194/egusphere-2026-2458
Preprint. Discussion started: 30 April 2026

3 Results

A full tabulation of results is available in Table S2 of the supplement and mirrors the results shown in the figures below along with coating thickness estimates and percentage of particles that are self-nucleated in each experiment. Spectra of activation fractions, as a function of temperature and S_{ice}, are provided for limonene-derived BSOA (Figure S3) and α-pinene-derived BSOA (Figure S4).

3.1 Ice nucleation experiments

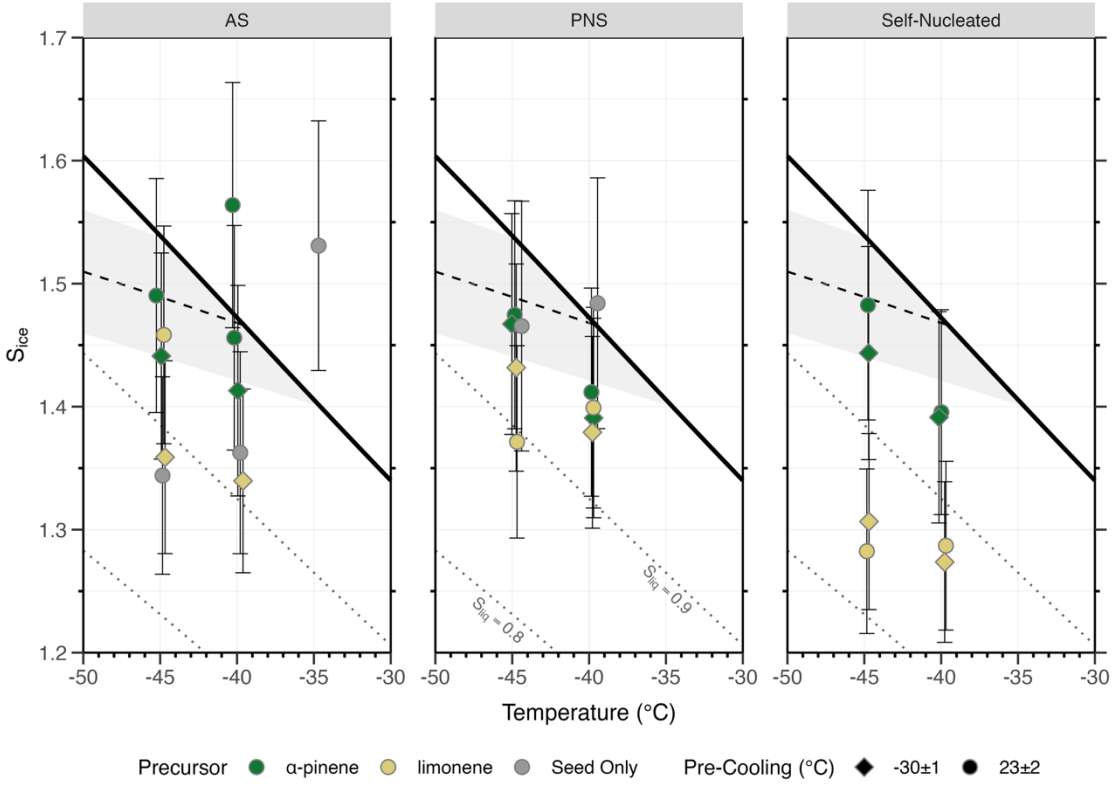

Figure 3 – Summary of thermodynamic onset conditions (T and S_{ice}) for an activation fraction of 0.5% of particles for all experiments conducted. Panels are separated and labelled according to sulfate seed particle or whether only self-nucleated particles were present. Colors indicate the precursor VOC used in generating BSOA or if bare seed particles were examined. Shapes indicate average pre-cooler temperature. Vertical error bars indicate the uncertainty in S_{ice} at onset of freezing. Shape width represents error in lamina temperature. Solid black line is water saturation i.e. S_{liq} = 1 with dotted black lines representing constant S_{liq} ratios. Dashed black line is the homogeneous freezing threshold of 100 nm diameter solution droplets as defined by (Koop et al., 2000), with uncertainty in water activity (a_w) of ±2.5% represented by the gray shaded region (Koop, 2004). Variability in heterogeneous activation fractions for BSOA experiments are provided by Figure S1.

3.1.1 Sulfate salts

PNS particles only nucleated ice consistent with homogeneous freezing of ABS at both -45°C and -40°C (Cziczo and Abbatt, 2001). For these homogeneous freezing experiments, the PNS particles were generated from a fresh ABS solution prior to all other experiments. AS nucleated ice heterogeneously at -45°C and -40°C (Abbatt et al., 2006). An onset of ice formation at -35°C was also observed for AS at high S_{ice} = 1.53±0.10 and was confirmed to be ice rather than droplet breakthrough by

https://doi.org/10.5194/egusphere-2026-2458
Preprint. Discussion started: 30 April 2026

depolarization measurements. 13% of sulfate particles on average were doublets and the influence of increased surface area on early freezing was not detected.

3.1.2 α-Pinene-derived BSOA experiments

Experimental results show that α-pinene-derived BSOA only nucleated ice heterogeneously at -40°C. This behavior was observed for α-pinene-PNS BSOA, α-pinene-AS BSOA, and self-nucleated α-pinene-derived BSOA. In all cases of heterogeneous freezing, a high S_{ice} was required. The lowest heterogeneous onset for α-pinene-PNS BSOA particles was S_{ice} = 1.39±0.08 at -39.7±0.4°C. Compared to the corresponding AS experiment, the coated 300 nm PNS particles had slightly better ice nucleation ability but well within error estimates (Figs. 3 and 5). The highest observed onset conditions were for room temperature α-pinene-AS BSOA particles (S_{ice} = 1.56±0.10, T = -40.3±0.4°C) and corresponded to a 6 nm coating, below the targeting coating thickness of 10 nm. For the same conditions, a sequential experiment showed that when a 20 nm layer was achieved, the onset of freezing (S_{ice} = 1.46±0.09) was within the homogeneous freezing regime of a 317 nm particle (S_{ice} = 1.46±0.05). Mean coating thickness for all α-pinene-derived BSOA coating experiments was 20.3±8.7 nm, where the error is one standard deviation from the mean, and had a full range of 6 – 34 nm. We note that the error in S_{ice} for every measurement of α-pinene-derived BSOA intersected the uncertainty range in homogeneous freezing for 100 nm aqueous solution droplets to some extent. For every α-pinene-derived BSOA experiment where pre-cooling was performed (-30±1°C), lower S_{ice} was required to nucleate ice in comparison to the corresponding room temperature (23±2°C) experiment. We also note that for α-pinene-PNS BSOA, ice formation at a threshold of 0.5% AF was nearly always proceeded by an onset of water uptake (also 0.5% AF), indicating a core-shell morphology likely formed where rapid surface liquefaction occurred prior to freezing seen before in the SPIN (Rapp et al., 2025b).

3.1.3 Limonene-derived BSOA experiments

Limonene-derived BSOA nucleated ice heterogeneously with the only exception being homogeneous freezing for the room temperature experiment for limonene-AS BSOA at -45°C. Ice nucleation for room-temperature limonene-AS BSOA at -40°C was observed but did not exceed the 0.5% AF threshold. Coating thickness of the seed particles ranged from 12 – 30 nm with a mean of 22.9±6.34 nm where the error is one standard deviation from the mean. No clear delineation between pre-cooling experiments was observed for self-nucleated and PNS experiments; however, for AS particles, only pre-cooled experiments showed heterogeneous ice nucleation. Specifically, instances of freezing for limonene-AS BSOA were (S_{ice} = 1.36±0.08, T = -44.7±0.4) and (S_{ice} = 1.34±0.07, T = -39.6±0.4) for coating thicknesses of 21 and 27 nm, respectively. Self-nucleated limonene-derived BSOA freezing onsets required lower S_{ice} than all other experiments (1.27±0.07 < S_{ice} < 1.31±0.07), including control experiments with effloresced AS. For all self-nucleated limonene-derived BSOA experiments, the error bars were at least 0.1 S_{ice} below the lower uncertainty range of the homogeneous freezing threshold. Heterogeneous ice nucleation efficiency for limonene-AS BSOA was within the same range as uncoated AS seeds. Unlike α-pinene-derived BSOA, water uptake reaching 0.5% AF was not observed for any limonene-derived BSOA experiment (see Table S2).

3.2 Aerosol chemical composition

Mass spectra obtained from PALMS-NG were averaged after selection of coated singlet particles (~ 320 – 350 nm) using aerodynamic vacuum diameter (Figure S2). Ions larger than m/z ±100 were not observed in the averaged mass spectra for all particles due to their infrequent detection. Minor differences were observed between sulfate seed for the same precursor, with the largest differences occurring between precursors. Specific ion fragment differences are shown in Figure S2. By applying the sampling and data processing methods described in Section 2.4.2 for AMS, the bulk oxygen to carbon (O:C) and hydrogen to carbon (H:C) ratios were derived and listed in Table 2. These bulk elemental ratios varied only slightly across different seed particles for the same VOC precursor, indicating that the overall oxidation state of the SOA coating remains broadly comparable under the different experimental conditions. The results suggested that differences in seed particle acidity do not substantially alter the reaction pathways within our experimental setup as measured by VIA-Vocus-CIMS. As OS formation has been observed to be highly sensitive to seed particle acidity (Cooke et al., 2024), this result in context with our experimental design is discussed in more detail in Sect. 4.1.

https://doi.org/10.5194/egusphere-2026-2458
Preprint. Discussion started: 30 April 2026

OS products were detected and assigned at the molecular-formula level using the VIA-Vocus-CIMS during the thermal desorption in all coating experiments with AS and PNS seed aerosols. A summary of chemical formulae of detected OS products is given in Table S3. Two OS formulas were observed from α-pinene-derived BSOA experiments with signal dominated by $C_8H_{16}O_6S$, while limonene experiments exhibited a broader OS formula coverage dominated by $C_8H_{18}O_5S$. Notably, under PAM oxidation conditions, the monoterpene carbon backbone likely undergoes oxidation fragmentation (Zhang et al., 2018), and the dominate OS and CHO species predominantly contain less than 10 carbon atoms. There are OS formulas overlap across different VOC precursors. However, as our measurements resolved composition at the molecular formula level, the overlaps do not imply identical OS structures. Within the same VOC precursor system, the OS formula families were similar between two seeds.

3.3 Physicochemical properties

As described in Sect. 2.5, the thermogram was obtained by increasing the temperature of VIA with a stable SOA source generated with PAM. The high mass resolution of Vocus-CIMS (up to 11000 FWHM) resolving power) allowed for sub-nominal separation of chemical formulae, and the thermograms for individual ion signals were obtained. By assuming the same sensitivity, overall bulk $T_{g,org}$ for the SOA coating was calculated as shown in Table 2. Parameterized values for $T_{g,org}$ and $\kappa_{O:C}$ were obtained using the methodology referenced in Sect. 2.5.

Table 2 – Physicochemical properties measured or parameterized using AMS, VOCUS, and VIA measurements.

Seed Particle	Gas-phase precursor	Thermogram $T_{g,org}$ (°C)	Parameterized $T_{g,org}$ (°C)	O:C AMS	H:C AMS	NH_4:SO_4 AMS	$\kappa_{O:C}$
PNS	α-pinene	-51.15±0.30	-24.15±21	0.21±0.007	1.27±0.01	1.66±0.04	0.068±0.008
PNS	limonene	-50.15±1.40	-32.15±21	0.23±0.004	1.25±0.01	1.60±0.06	0.071±0.009
AS	α-pinene	-65.15±0.65	-96.15±21	0.20±0.003	1.27±0.01	2.12±0.04	0.066±0.008
AS	limonene	-79.15±0.93	-97.15±21	0.23±0.002	1.27±0.01	2.09±0.05	0.071±0.009
-	α-pinene	-61.15±0.30	-91.15±21	0.21±0.003	1.26±0.01	-	0.068±0.008
-	limonene	-69.15±1.00	-77.15±21	0.21±0.003	1.27±0.01	-	0.068±0.008

Thermogram- and parameterized-derived $T_{g,org}$ values were lower than the pre-cooling temperature of -30±1°C with the only exception being the parametrized estimate for α-pinene-PNS particles -24.15±21°C. There was wide variation in both thermogram and parameterized $T_{g,org}$. Within our study, thermogram-derived $T_{g,org}$ values have a pair-wise difference of -7±24.5° from parameterized (standard error of the difference). From these measurements and estimates, it is to be inferred that nearly all BSOA examined were in a liquid phase state. O:C and H:C ratios were very similar for all BSOA, ranging from 0.20 to 0.23 and 1.25 to 1.27, respectively. As O:C were similar, the derivative product $\kappa_{O:C}$ was also similar across experimental combinations, with a value of ~0.07. The observed AMS O:C ratios are indicative of freshly generated BSOA with minimal atmospheric aging, closely resembling SOA measured at the Hyytiälä boreal forest research site where AMS O:C ratios ranged from 0.22 to 0.23 (Finessi et al., 2012; Raatikainen et al., 2010). We also observed NH_4:SO_4 ratios inconsistent with the expected molar ratio of ABS (i.e., 1:1); rather, they more closely matched those of letovicite $(NH_4)_3H(SO_4)_2$ which has a NH_4:SO_4 molar ratio of 1.5.

3.4 Multimodal analysis

A summary of the multimodal analysis for each coating experiment is given in Table 3. Overall, self-nucleation was frequently observed for α-pinene-PNS BSOA experiments, despite using the same operating procedures for corresponding AS experiments. The percentage of singlets to doublets across all experiments was similar, with a mean value of 87.22 ± 2.7%, where uncertainty is one standard deviation from the mean. A full tabulation of unaveraged data specific to each isothermal lamina temperature of the SPIN is provided in Table S2.

https://doi.org/10.5194/egusphere-2026-2458
Preprint. Discussion started: 30 April 2026

Table 3 – Multimodal fitting results for the eight coating experiments performed. The first three columns indicate the experimental combination of seed particle, gas-phase precursor, and pre-cooling temperature and correspond to the particles plotted in Figure 3.

Seed Particle	Gas-phase precursor	Pre-cooling temperature (°C)	Self-Nucleated (%)	Singlet/Doublet (%)
PNS	α-pinene	−30±1	28.2±35.7	85.0±0.0593
PNS	α-pinene	23±2	22.6±7.57	85.9±0.0530
PNS	limonene	−30±1	0.427±3.44	87.9±0.140
PNS	limonene	23±2	0.515±5.39	89.0±0.0696
AS	α-pinene	−30±1	8.18±10.1	85.5±0.0878
AS	α-pinene	23±2	0.364±2.71	86.3±0.0718
AS	limonene	−30±1	1.12±2.71	86.9±0.109
AS	limonene	23±2	0±1.24	88.7±0.0632

3.5 Statistical testing

Normality of the measured onset S_{ice} values was evaluated using the Shapiro-Wilk test, indicating no statistically significant deviation from a normal distribution ($W = 0.96$, $p = 0.517$). A four-way analysis of variance (ANOVA) was conducted to quantify the contribution of precursor VOC, seed particle type (including self-nucleated), pre-cooling, and SPIN lamina temperature to variability in onset S_{ice}. The variables were initially tested additively (i.e., assumption of no cross-variable interactions). Among the variables tested, only the application of pre-cooling did not have a statistically significant effect ($p = 0.14$). Precursor VOC identity had the most significant effect on onset S_{ice} ($F(1, 16) = 25.74$, $p < 0.001$). This was followed by effects caused by seed particle ($F(2, 16) = 6.06$, $p < 0.05$) and SPIN lamina temperature ($F(1, 16) = 5.11$, $p < 0.05$). The cross-interaction effect of seed particle and precursor VOC on onset S_{ice} was also tested and found to be insignificant ($p = 0.28$). Post hoc pairwise Student's t-testing of the ANOVA results found the mean difference in onset S_{ice} for α-pinene- and limonene-derived BSOA particles remained statistically significant ($\Delta\mu = 0.086$, $t(10) = 5.22$, $p < 0.001$) but was insignificant for PNS vs. AS seed particles ($\Delta\mu = -0.023$, $t(6) = -1.22$, $p = 0.27$). For self-nucleated particles, there was a statistically significant difference between S_{ice} observed and predicted by homogeneous freezing thresholds ($t(7) = -2.51$, $p < 0.05$).

4 Experimental uncertainties

4.1 Particle acidity and OS formation

In this study, the selection of ABS salt, rather than an equimolar mixture of AS and H_2SO_4, was motivated by the need to accurately characterize homogeneous ice nucleation within the SPIN. The degree of neutralization in ammoniated sulfate has been shown to significantly affect ice nucleation ability (Bertozzi et al., 2024), thus the use of an ABS standard was preferred. However, this choice also influences OS formation. Previous work has demonstrated that for IEPOX-derived SOA, HSO_4^- is approximately two orders of magnitude less effective than SO_4^{-2} as a nucleophile (Cooke et al., 2024), implying the use of ABS may suppress both acid-catalyzed SOA yield and OS formation.

Additionally, partial neutralization of the ABS seed particles by ammonia was observed in our experiments as indicated by the NH_4:SO_4 AMS ratio of 1.6 rather than the expected value of 1.0 for ABS. While the source of ammonia is uncertain, we speculate that the use of dry filtered room air to balance flows and pressure (Fig. 1) may have contributed. Regardless of this uncertainty, we observed homogeneous freezing of "fresh" PNS consistent with ABS (Cziczo and Abbatt, 2001). This was the first experiment performed, suggesting that neutralization was gradually changing.

https://doi.org/10.5194/egusphere-2026-2458
Preprint. Discussion started: 30 April 2026

4.2 Chemical characterization of OSs

Composition and quantification of OS formed by α-pinene and limonene has traditionally been performed using liquid chromatography electrospray ionization-mass spectrometry (LC/ESI-MS) (Iinuma et al., 2007a, b; Surratt et al., 2007, 2008). LC/ESI-MS is a soft ionization technique shown to preserve molecular structure of BVOC-derived OS through analysis of authentic standards (Staudt et al., 2014). In contrast, the VIA-Vocus CIMS methodology involves thermal desorption and may induce decomposition and/or chemical alteration of OS. This likely contributes to the lack of agreement in OS composition between this study (Table S3) and previous LC/ESI-MS measurements (Iinuma et al., 2007a, b; Surratt et al., 2007, 2008). A comprehensive evaluation of VIA-Vocus CIMS for OS characterization and quantification requires analysis of authentic BVOC-derived OS standards and is beyond the scope of this study. Thus, the results presented here should be interpreted with this limitation in mind.

5 Discussion

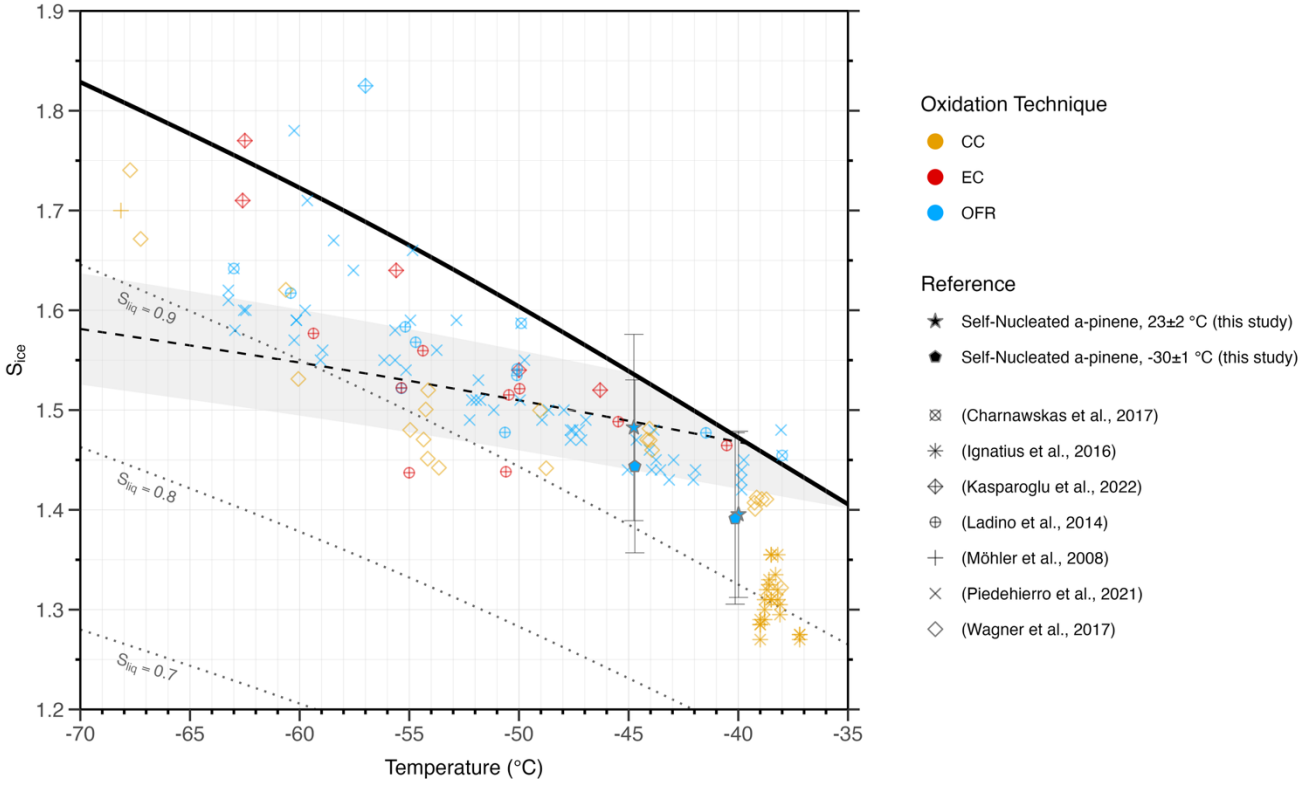

Figure 4 – Summary of thermodynamic onset conditions (T and S_{ice}) for self-nucleated α-pinene BSOA particles. Colors indicate the oxidation technique used to generate BSOA: cloud chamber (CC), environmental chamber (EC) and oxidation flow reactor (OFR). Shapes denote either the reference values or results obtained in this study. Uncertainties in both T and S_{ice} for results from this study are the same as in Fig. 3, with an activation fraction (AF) onset threshold of 0.5%. Uncertainties were omitted for reference values to accommodate the density of data presented. Similarly, the oxidant type used is omitted for simplicity in assigning shapes. Lines and shading are identical to those from Fig. 3. AF thresholds used to define the onset of ice formation (when applicable) varied across referenced studies, including 1%, 5%, and 10% (Ignatius et al., 2016); 0.5% (Kasparoglu et al., 2022); 0.1% (Ladino et al., 2014; Wagner et al., 2017); and 1% (Möhler et al., 2008; Piedehierro et al., 2021).

https://doi.org/10.5194/egusphere-2026-2458
Preprint. Discussion started: 30 April 2026

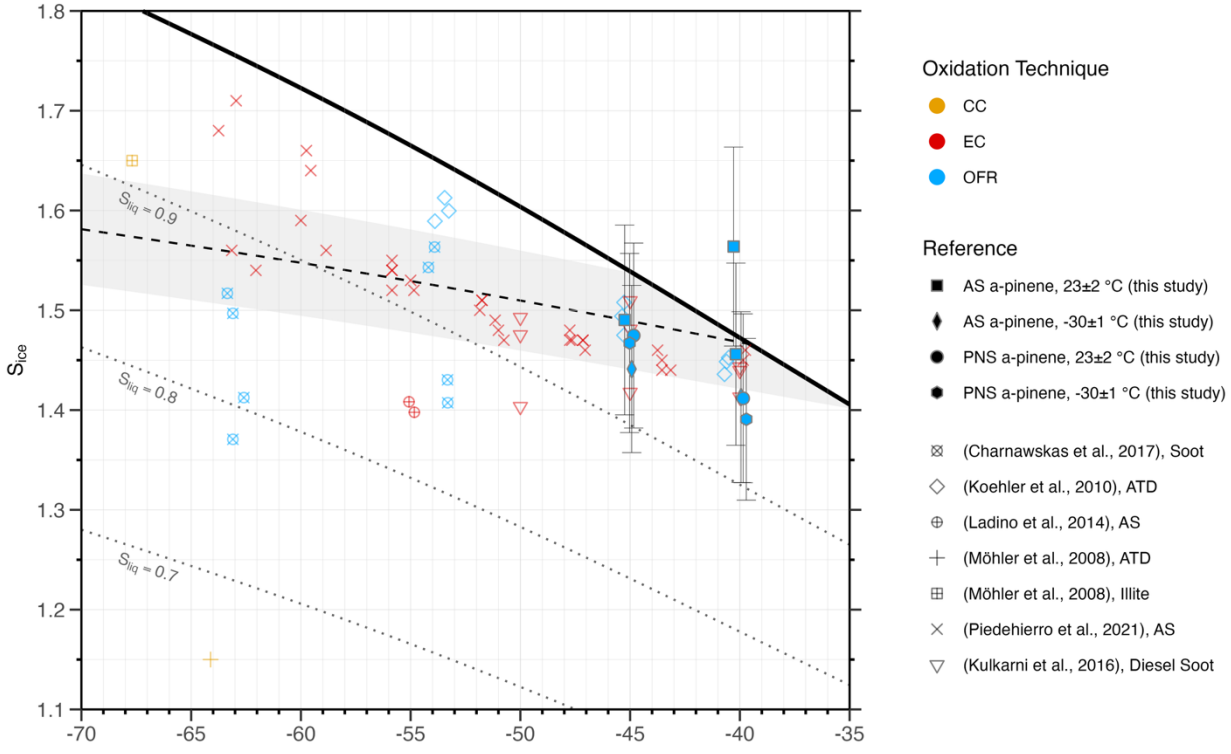

Figure 5 – Summary of thermodynamic onset conditions (T and S_{ice}) for coated or internally mixed α-pinene SOA particles. All datapoints are BSOA coated material with the exception of (Ladino et al., 2014). Colors indicate the oxidation technique used to generate BSOA: cloud chamber (CC), environmental chamber (EC) and oxidation flow reactor (OFR). Shapes denote either the reference values (including respective seed particle composition) or results obtained in this study. Uncertainties in both T and S_{ice} for results from this study are defined the same as in Fig. 3, with an activation fraction (AF) onset threshold of 0.5%. Uncertainties were omitted for reference values to accommodate the density of data presented. Similarly, the oxidant type used is omitted for simplicity in assigning shapes. Lines and shading are identical to those from Fig. 3. AF thresholds used to define the onset of ice formation (when applicable) varied across referenced studies, including 0.1% (Ladino et al., 2014); and 1% (Koehler et al., 2010; Kulkarni et al., 2016; Möhler et al., 2008; Piedehierro et al., 2021).

5.1 Factors influencing the ice nucleation ability of SOA

5.1.1 Precursor identity

Our results showed the ice nucleating abilities of BSOA have a strong dependence on precursor VOC identity with both ANOVA and pairwise Student's t-test showing significance ($p < 0.001$). This precursor composition dependence has been observed in the SPIN with proxy SOA ice nucleation measurements (Rapp et al., 2025b), which showed no ice nucleation ability for proxy OS salts but citric acid nucleated ice effectively in agreement with previous work (Murray et al., 2010). It is worth noting that the OS identified in this study have a higher degree of oxygenation in comparison to the OS salts in previous work. While our results were limited to limonene and α-pinene, this speciation effect is evident in literature. Charnawskas et al. (2017) measured the ice nucleating properties of longifolene-, α-pinene-, and naphthalene-derived SOA across a broad range of conditions and noticed a clear difference between the three VOCs, specifically naphthalene performing best. In contrast, Kasparoglu et al. (2022) measured ice nucleating properties of SOA derived from eleven unique biogenic and

https://doi.org/10.5194/egusphere-2026-2458
Preprint. Discussion started: 30 April 2026

anthropogenic VOCs with no heterogeneous freezing onsets observed, including limonene, naphthalene, and α-pinene, which indicates some other variation between experimental studies must be responsible. Our results for self-nucleated α-pinene SOA are consistent with literature values, demonstrating they require high ice saturation and low temperatures to nucleate ice. The only exception we identified are the results by Ignatius et al., (2016) as shown in Figure 4, which also achieved a remarkable 10% AF for some experiments. In summary, α-pinene-derived BSOA particles are largely homogeneous nuclei and at best, poor heterogeneous nuclei. However, limonene-derived BSOA particles are moderately effective INP (see Fig. 6) with efficiencies like AS which has been observed for other proxy SOA (Schill and Tolbert, 2013).

Figure 6 – Summary of thermodynamic onset conditions (T and S_{ice}) for self-nucleated and limonene BSOA coated sulfate particles. Colors indicate the oxidation technique used to generate SOA: cloud chamber (CC) or oxidation flow reactor (OFR). Shapes denote either the reference values or results obtained in this study. Uncertainties in both T and S_{ice} for results from this study are the same as in Fig. 3, with an activation fraction (AF) onset threshold of 0.5%. Uncertainties from literature values were included as available. Lines and shading are identical to those from Fig. 4. AF thresholds used to define the onset of ice formation for reference values were 0.5% (Kasparoglu et al., 2022) and 0.1% (Wagner et al., 2017).

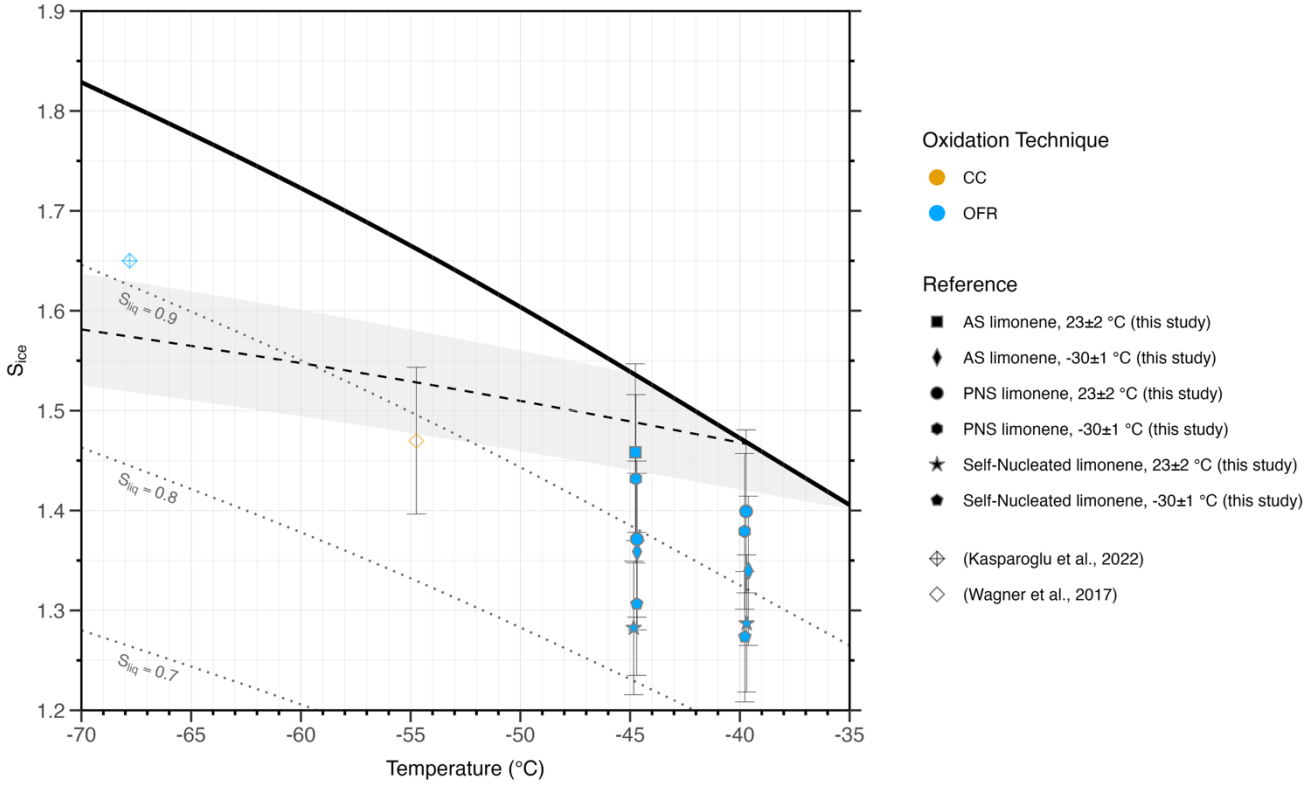

5.1.2 Oxidants

Combining our results with the existing literature on α-pinene-derived BSOA, we find no systematic relationship between ice nucleation ability and either the dominant oxidant (O_3, OH, hν) or the oxidizing environment (i.e., OFR, CC, or EC). The α-pinene-derived BSOA particles and coatings generated in this study were produced in an OFR comparable to those used in previous work (Charnawskas et al., 2017; Piedehierro et al., 2021) and exhibited similar ice nucleation onsets (Figs. 4 and 5). Moreover, OFR studies showed largely consistent behavior with experiments conducted in ECs (Kasparoglu et al., 2022;

https://doi.org/10.5194/egusphere-2026-2458
Preprint. Discussion started: 30 April 2026

Ladino et al., 2014) and CCs (Möhler et al., 2008; Wagner et al., 2017), with the notable exception of Ignatius et al., (2016). Residence time of reactions within OFRs (timescale of minutes) will differ from those in EC/CC chambers (timescale of hours). In the case of examining the ice nucleating properties of particles derived from multiphase reactions, comparing oxidizing environment becomes more nuanced as limitations in chemical kinetics become more pronounced. In the context of the studies cited previously, our findings suggest that differences in oxidizing environment are unlikely to explain the small variations in ice nucleation ability reported across studies, particularly for self-nucleated particles.

Intercomparison based on oxidant type leads to a similar but less certain conclusion due to variation among studies in whether oxidation was dominated by O_3 or $^{\bullet}OH$ (see Introduction) and at different concentrations. If oxidant identity were a primary driver of ice nucleation properties for a given precursor, larger variability in onset saturation would be expected for both self-nucleated α-pinene-derived BSOA (Fig. 4) and sulfate aerosol particles coated with α-pinene-derived BSOA (Fig. 5). Instead, onset conditions cluster closely across studies, reinforcing the importance of precursor-specific effects on SOA ice nucleation (Sect. 5.1.1) rather than oxidant. A clear example is provided by Piedehierro et al. (2021), who explicitly compared dry ozonolysis, wet ozonolysis, and wet $^{\bullet}OH$ photooxidation in an OFR, and observed similar ice nucleation onsets near or above the homogeneous freezing threshold (Koop et al., 2000). Our results using O_3/$^{\bullet}OH$ oxidation, albeit at different concentrations, were consistent with these findings, with coated and self-nucleated α-pinene-derived BSOA exhibiting comparable onset ice saturations. Our results are most similar to those shown by Wagner et al. (2017), which obtained a unimodal distribution of self-nucleated SOA with approximate median mobility-equivalent diameter of 300 nm, very comparable to our coated particles. This similarity was despite the different oxidants present and ice nucleating measurement technique (see Sect. 5.1.6).

Additional support comes from Kulkarni et al. (2016), where NO_x was present during $^{\bullet}OH$ oxidation of α-pinene-derived BSOA coatings on diesel soot, yet ice nucleation behavior closely resembled that reported by Charnawskas et al. (2017), in which soot coated with $^{\bullet}OH$ oxidized α-pinene-derived BSOA acted as poor heterogeneous or predominantly homogeneous ice nuclei. Although our self-nucleated α-pinene-derived BSOA results were the closest to Ignatius et al. (2016) among existing studies, attributing this similarity to $^{\bullet}OH$ oxidation alone is unlikely given the stronger agreement with Wagner et al. (2017), which employed exclusively O_3 oxidation. This is further corroborated by Ladino et al. (2014) where aqueous $^{\bullet}OH$ photooxidation of the water-soluble organic fraction of α-pinene ozonolysis products were similar to pure ozonolysis products.

While oxidant identity does not demonstrate a significant direct effect on the ice nucleation ability for α-pinene-derived BSOA, oxidants may exert an indirect influence by modifying particle phase state. In the case of α-pinene, ozonolysis yields oligomerized products (Tolocka et al., 2004) which can increase viscosity (Grayson et al., 2017). Oxidant-dependent changes in phase state have been demonstrated in laboratory studies; for example, $^{\bullet}OH$ oxidation of guaiacol produces lower-viscosity SOA than $NO_3^{\bullet}$ oxidation, with the latter remaining highly viscous over a wide range of relative humidities and temperatures (Nikkho et al., 2024). Similarly, $NO_3^{\bullet}$ oxidation of catechol surprisingly yields crystalline SOA, whereas O_3 oxidation does not (Mahrt et al., 2025). Taken together, current evidence suggests that oxidants influence ice nucleation properties primarily through their impact on SOA phase state rather than through direct compositional effects (see Sect. 5.1.4).

5.1.3 O:C ratio

Our study also strengthens an argument against O:C being responsible for discrepancies in ice nucleation ability for self-nucleated SOA particles. As noted by Ladino et al. (2014), oxidative age was not enough to explain the differences between systems and suggested that "detailed composition of particles is not of paramount importance to their ice nucleating abilities". Similarly, a minor difference using O:C was noted by Piedehierro et al. (2021) in the O:C range of 0.45–1.1. For soot particles coated with various O:C ratios of α-pinene-derived BSOA, Charnawskas et al., (2017) noted that lower O:C ratios (0.42 – 0.45) nucleated ice more efficiently than higher ratios (0.59 - 0.64). The opposite trend was determined for naphthalene-derived SOA but was attributed as an effect of O:C on the T_g of each SOA. For monocarboxylic acids, it was determined O:C ratio had a pronounced effect on heterogeneous ice nucleation activity in the range of 0.3 - 0.5 (Schill and Tolbert, 2012). For this study, we focused on achieving a comparable SOA-coating thickness rather than explicitly testing oxidative age, and as such, the degree of atmospheric aging for α-pinene and limonene differ by about 3 days but the O:C ratios were highly similar (0.21 – 0.23). In comparison to the O:C of literature values, we note ours are below the range defined by Schill and Tolbert (2012).

https://doi.org/10.5194/egusphere-2026-2458
Preprint. Discussion started: 30 April 2026

Wagner et al. (2017) argued the difference between their results and Ignatius et al. (2016) was due to O:C ratio, which was 0.25 compared to 0.35, respectively. We note that self-nucleated α-pinene-derived BSOA in this study had a similar O:C ratio as Ignatius et al., (2016), but more closely resembled results from Wagner et al. (2017), contradicting the argument for O:C being responsible. If O:C influences the ice nucleating behavior of BSOA by modifying particle composition, it is not supported by our results or clear from literature data for atmospherically relevant particles. When considering prior work on ice nucleation of simple sulfate esters (Rapp et al., 2025b), we agree with the finding of Charnawskas et al., (2017) that O:C is important to ice nucleation insomuch as it modifies particle phase.

5.1.4 Aerosol phase state and T_g

Given T_g is an accurate predictor of a glassy phase state and only glassy amorphous solids or highly viscous semi-solids nucleate ice heterogeneously, we would expect only two of our twelve experimental combinations (see Table 2, size unique chemical combinations with and without pre-cooling) to nucleate ice heterogeneously. Specifically, pre-cooled (−30±1°C) α-pinene- and limonene-PNS BSOA particles should nucleate ice heterogeneously, as their O:C parameterized $T_{g,org}$ of −24.15°C and −32.15°C indicate glassy and semi-solid phase states, respectively. This expectation of ice nucleation assumes that $T_{g,org} \cong T_g$ and is an upper bound. These two compounds did nucleate ice heterogeneously at the 0.5% activation threshold as expected (see Fig. 3); however, so did nine other experimental combinations. According to both measured and predicted values of $T_{g,org}$, these particles should be in a liquid phase, with a minimum difference in PCU temperature being 31.85°C warmer than $T_{g,org}$ and maximum of 122.15°C (assuming completely dry conditions), suggesting even a semi-solid phase is unlikely.

This disparity in observed vs. predicted ice nucleating behavior cannot be unambiguously attributed to measurement uncertainty in SPIN. Onset quantification was performed using highly conservative metrics, with lamina saturation uncertainty accounting for error propagation in both flow and temperature (Rapp et al., 2025b). Lamina uncertainty was intentionally unaveraged to purposefully impose an accuracy penalty associated with random error, thereby representing a "worst-case" uncertainty estimate. Systematic lamina errors were constrained using AS and PNS control experiments, which served as calibration standards. Potential misclassification of heterogeneous freezing as "early" homogeneous freezing was addressed through monodisperse AN control experiments and by calculating lamina ice saturation from cold points within the chamber, as described in Sect. 2.6.2. Furthermore, a comprehensive description of uncertainty for the SPIN instrument (Garimella et al., 2017) details we are very likely *underestimating* particle counts by a factor of 2.86 if we had used the mean correction factor of 4 to account for particle loss by lamina spreading.

Attributing unexpected heterogeneous freezing results to uncertainty in $T_{g,org}$ estimates is also unlikely as we utilized two values for comparison (i.e. measured and parameterized based on AMS measurements). First, $T_{g,org}$ derived from VIA-Vocus CIMS measurements has been performed for α-pinene-derived BSOA previously (Niu et al., 2025) and agreed with existing measurements (Grayson et al., 2016; Renbaum-Wolff et al., 2013; Zhang et al., 2015) and models (DeRieux et al., 2018). We note that thermogram measurements account for both volatility and chemical composition of the generated compounds, whereas parameterized values are limited to number of carbon, hydrogen, and oxygen atoms present (see Sect. 2.1 of DeRieux et al., 2018). The compound specific nature of the thermogram measurements increases the confidence of these measurements. However, we acknowledged that the VIA-Vocus CIMS measurements may not provide a complete molecular coverage of SOA due to ionization selectivity bias and thermal desorption may induce dehydration and fragmentation for selected compounds (see Sect. 4.2.). Despite the limitations, our main conclusions rely on relative differences between experiments obtained under identical operating conditions, and on agreement between thermogram-derived trends and the independent parametrized T_g estimation. Therefore, the potential incomplete coverage is unlikely to reverse the inferred conclusion.

These findings also corroborate the conclusion made by Kasparoglu et al. (2022) that "a glassy phase state may be necessary but is not a sufficient criterion for particles to freeze heterogeneously". Conversely, their study did not observe heterogeneous freezing for glassy particles as expected and determined viscosity using the dimer coagulation isolation and coalescence technique (Rothfuss and Petters, 2016). Here we observe heterogeneous freezing for particles inferred to be liquid based on $T_{g,org}$. Based on the general consensus in the literature that only glassy or semi-solid particles nucleate ice heterogeneously, our results suggest either (1) that $T_{g,org}$ is not a reliable predictor of aerosol phase state for these BSOA and, by extension, a priori

https://doi.org/10.5194/egusphere-2026-2458
Preprint. Discussion started: 30 April 2026

ice nucleation ability, or (2) that aerosol phase state alone is insufficient to predict ice nucleation. We argue that the former explanation is more likely as pre-cooling was observed to decrease onset S_{ice} compared to corresponding room temperature experiments for all α-pinene-derived BSOA experiments (within S_{ice} error) and unambiguously for limonene-AS BSOA (outside error or absence of room-temperature onset for -40°C limonene-AS BSOA). Recent analysis has also clearly shown aerosol phase state does enhance heterogeneous ice formation (Li et al., 2024).

5.1.5 Coating thickness

Coating thickness did not appear to influence ice nucleating ability. For the experiment with the thinnest coating, 6 nm for α-pinene-AS BSOA, we would expect onset of freezing to share similarities to bare AS particles if an incomplete coating was present (Cziczo et al., 2009; Möhler et al., 2008). Instead, we observed homogeneous freezing at high S_{ice}. Repeating the experiment with a thicker coating showed homogeneous freezing again at a lower onset but still within error of the previous measurement. This result indicates particles were fully coated even at the minimum observed coating of 6 nm. As described in 3.1.3, pre-cooled limonene-AS BSOA nucleated ice at similar onset conditions as uncoated AS. However, self-nucleated limonene nucleated ice as efficiently or better than AS despite being smaller in diameter – indicating the coating was responsible for the onset, not the seed particle. Combining these results, we are confident that heterogeneous freezing of coated AS was not due to uncoated activation sites, but we caution that without direct TEM/SEM observations we cannot be certain.

5.1.6 Inherent instrumentation bias

Differences among BSOA ice nucleation studies have been attributed in part to instrumental biases, particularly those arising from the mechanisms used to observe freezing. Wagner et al. (2017) suggested that discrepancies between AIDA expansion measurements and SPIN-CFDC results (Ignatius et al., 2016) stem from differences in humidification rate and particle residence time. The long residence times in AIDA allow particles to equilibrate with chamber conditions, promoting liquefaction of BSOA and leading primarily to homogeneous freezing. In contrast, CFDCs have short residence times (e.g., ~ 10 s) preventing the ability of organic particles to equilibrate before freezing (Piedehierro et al., 2021), increasing the likelihood of observing heterogeneous freezing. Numerical diffusion modeling supports this non-equilibrium assumption for SPIN (Rapp et al., 2025b), although equilibration depends strongly on particle hygroscopicity and phase state; highly hygroscopic particles ($\kappa \gtrsim 0.4$) rapidly uptake water and liquefy. Notably, limonene-derived BSOA in this study did not exhibit the water uptake features observed for α-pinene-derived BSOA or in prior proxy SOA work (Rapp et al., 2025b), despite nearly identical residence times and humidification rates. This indicates that heterogeneous freezing cannot be explained by instrumental operation alone, rather a combination of the former effects and physicochemical properties of the particles.

If instrumentation were the primary cause of discrepancies in α-pinene-derived BSOA results, our self-nucleation measurements would be expected to align with previous SPIN studies (Ignatius et al., 2016; Piedehierro et al., 2021), particularly by Ignatius et al. (2016). Both studies employed SPIN, pre-cooled particles, PAM-OFR oxidation with similar oxidants (O_3, $^{\bullet}OH$, hν), and produced comparable O:C ratios (0.23 vs. 0.25). In the absence of direct measurements, O:C is commonly used to estimate physicochemical properties such as $T_{g,org}$ and κ (DeRieux et al., 2018; Lambe et al., 2011b; Shiraiwa et al., 2017), parameters to which SPIN modeling has shown strong sensitivity (Rapp et al., 2025b). Nevertheless, our results more closely resemble those from AIDA (Wagner et al., 2017). Although our generous uncertainty ranges encompass much of the data from Ignatius et al. (2016), we did not observe comparably high activation rates, which we attribute most likely to the larger particle diameters used in their study.

Finally, pre-activation of organic aerosol via pre-cooling has been proposed as a mechanism for enhanced ice nucleation (Ladino et al., 2014). Our results do not support this hypothesis as we observed heterogeneous freezing of room-temperature limonene-derived BSOA performing similarly to pre-cooled. Under the assumption of pre-activation, the pre-cooled should have exhibited improved ice nucleating properties but this difference was not observed.

https://doi.org/10.5194/egusphere-2026-2458
Preprint. Discussion started: 30 April 2026

5.2 Atmospheric implications

5.2.1 Freezing mechanisms

It is likely that either immersion or deposition freezing occurred in these experiments based on previously conducted numerical diffusion modelling of SPIN (Rapp et al., 2025b). This could explain a commonly observed feature for α-pinene-derived BSOA where particle diameters increased but did not achieve a depolarization ratio necessary for ice classification until at higher RH. This depolarization ($0.30 < \delta_{SPIN} < 0.35$) was slightly different from previous studies ($\delta_{SPIN} < 0.16$) examining more hygroscopic particles (Rapp et al., 2025b) where modeling suggested the particles were fully liquefied and as such, low depolarization is expected. Due to the lower modeled κ, full liquefaction is less likely if the particle is assumed to be in a glassy state, supporting the observed difference in δ_{SPIN}. Given the above, it is possible α-pinene-derived BSOA nucleated ice via immersion freezing. In contrast, a transitory period of water uptake to ice was not observed for limonene-derived BSOA (see Table S2), which was reminiscent of previous observations of glassy citric acid aerosol that numerical diffusion modeling indicated surface liquefaction of the particle would not happen within the residence time in the SPIN chamber (Rapp et al., 2025b).

5.2.2 Uncertain role of multiphase chemistry

A surprising finding in this work is that PNS particles, which we observed to nucleate ice homogeneously (Sect 3.1.1) and as seen in previous work (Cziczo and Abbatt, 2001), exhibit enhanced ice nucleating abilities when coated with α-pinene- or limonene-derived BSOA. This finding suggests that the coating effectively converts the particles from a primarily homogeneous to heterogeneous nuclei. In total, six heterogeneous onsets were observed with PNS seed particles compared to three with AS. While this result may superficially indicate that multiphase chemistry enhances ice nucleation efficiency, we caution that several complexities must be considered when interpreting the role of multiphase chemistry in this work.

First, the conservative uncertainty ranges for ice onsets of PNS coated particles overlap homogeneous freezing uncertainty in all cases. ANOVA statistical testing revealed when cross effects of seed particle and precursor VOC were combined, there was no significant effect ($p = 0.59$) while seeds alone did have a significant effect ($p < 0.01$). This however failed subsequent Student's t-test post hoc analysis ($p > 0.84$). The potential influence of self-nucleated BSOA particles must also be considered. In the case of α-pinene-derived BSOA, prominent self-nucleation makes it difficult to definitively isolate the effect of the coating, as evidenced by similar onset in the self-nucleation experiments at -40°C. However, this limitation is less significant for limonene-derived BSOA experiments, where minimal self-nucleation was identified.

Second, limonene-PNS BSOA was associated with the highest number of OS production (eleven) as observed by VIA-Vocus CIMS (see Sect. 4.2.), followed by limonene-AS BSOA (six). In comparison, only two OS were identified for α-pinene-derived BSOA coatings using VIA-Vocus-CIMS (see Table S3). This suggests that for our experimental conditions, limonene promoted OS formation more readily, particularly for PNS seeds. However, it is worth noting that the improved efficiency of self-nucleated limonene BSOA compared to coated PNS contradicts the hypothesis that OS formation via multiphase chemistry improves ice nucleating properties. This difference was within S_{ice} error for some measurements, prohibiting any qualifying statements. It is also uncertain whether VIA-Vocus-CIMS quantifies all OS formed, as LC/ESI-MS has traditionally been used in OS characterization and quantification in BSOA especially due to its soft ionization conditions (Surratt et al., 2007; Surratt et al., 2008; Inuma et al., 2007; Inuma et al., 2008). The 20–23-minute residence time for particle generation used in this study may also be insufficient to observe appreciable OS formation as seen in earlier chamber experiments (e.g., Surratt et al., 2008). Given the uncertainties in OS quantification and experimental constraints, we cannot definitively state whether OS formation via multiphase chemistry enhances heterogeneous ice nucleation of BSOA at this time. Furthermore, it has been recently shown for IEPOX-derived OS formation that a larger particulate fraction of HSO_4^- compared to SO_4^{2-} may inhibit OS formation due to HSO_4^- being a less effective nucleophile (Cooke et al., 2024). Future INP work should consider using acidified ammonium sulfate aerosol (instead of pure PNS particles) to examine if HSO_4^- versus SO_4^{2-} has more potential to form OS from α-pinene and limonene oxidation and thus possibly lead to more deposition ice nucleating BSOA.

https://doi.org/10.5194/egusphere-2026-2458
Preprint. Discussion started: 30 April 2026

6 Conclusions

This study investigated the deposition ice nucleating properties of α-pinene- and limonene-derived BSOA, including self-nucleated particles and BSOA coatings on AS and PNS seed particles for cirrus-relevant conditions (−45, −40, −35°C; $1.0 \leq S_{ice} \leq 1.6$). We tested several hypotheses addressing precursor-dependent ice-nucleating efficiency, the predictive capability of T_g in ice nucleation, the ice nucleating behavior of self-nucleated BSOA, and the influence of acid-driven multiphase chemistry. The principal findings are summarized as follows:

1. Gas-phase precursor identity emerged as the dominant control on BSOA ice nucleating properties ($p < 0.001$). Precursor chemistry exceeded influences of seed particle composition, inferred aerosol phase state, and freezing temperature. We also corroborated findings in previous studies that bulk O:C ratio is unimportant to ice nucleation directly but can indirectly influence phase state via water uptake.

2. Self-nucleated α-pinene-derived BSOA predominantly nucleated ice homogeneously, at or above the uncertainty bounds of homogeneous freezing, consistent with prior studies. In contrast, self-nucleated limonene-derived BSOA nucleated ice via heterogeneous freezing, with onsets comparable to crystalline AS. These results demonstrate that BSOA cannot be assigned a single ice nucleating efficiency; instead, precursor-specific chemistry must be explicitly considered in deposition ice nucleation.

3. T_g failed to reliably predict ice nucleation behavior for atmospherically relevant BSOA types. Heterogeneous ice nucleation was observed for particles inferred to be in a liquid state based on both measured and estimated T_g. These findings indicate in collection with previous research, that although high particle viscosity may facilitate heterogeneous freezing, phase state inferred from T_g alone is insufficient to predict ice nucleating ability. The application of pre-cooling was observed to lower the S_{ice} required for ice formation for all α-pinene-derived BSOA types and limonene-AS BSOA; however, pre-cooling overall did not show a statistical difference ($p > 0.05$), likely due to the small sample size.

4. The role of multiphase chemistry, including organosulfate formation, could not be conclusively isolated in this study especially due to the lack of offline chemical analyses by well-established LC/ESI-MS methods used to characterize organosulfate formation. More work is likely needed with authentic standards to characterize how stable organosulfates are in the VIA Vocus CIMS that measured organosulfate-containing BSOA components. PNS particles exhibited a transition from homogeneous to heterogeneous nuclei with BSOA coatings, regardless of precursor. Overall, more heterogeneous onsets were attributed to PNS seeds than AS. Uncertainties in onset S_{ice}, simultaneous presence of self-nucleated particles, and restricted reaction time preclude a definitive conclusion. As such, the role of multiphase chemistry in the ice nucleation of BSOA remains unresolved.

Collectively, these results highlight critical limitations in current metrics used to predict the organic ice nucleating properties under cirrus conditions. Metrics such as T_g or bulk O:C ratio are insufficient to explain the ice nucleating properties of BSOA. New comprehensive frameworks are needed to account for precursor-specific chemistry, viscosity, and non-equilibrium processes inherent to common ice nucleation instruments. Future studies should prioritize controlled multiphase chemistry experiments (i.e., possibly at longer reaction timescales), rigorous intercomparisons across ice nucleation instruments using identical aerosol populations, and the development of improved parametrizations suitable for climate model integration.

Data availability

Data will be made available to a Purdue University repository with a permanent DOI upon completion of peer-review

https://doi.org/10.5194/egusphere-2026-2458
Preprint. Discussion started: 30 April 2026

Author contributions

CNR prepared the manuscript with contributions from all co-authors. CNR and SN performed all investigative experiments and data analysis. CNR conducted formal analysis and collated results. CNR, SN, JDS, YZ, and DJC developed experimental methodology and project conceptualization. JDS, YZ, and DJC acquired funding for the project.

Competing interests

Jason D. Surratt is a member of the editorial board of Atmospheric Chemistry and Physics.

Financial support

This research has been supported by the National Science Foundation (grant nos. 2131369, 2131370, and 2131371) and the National Oceanic and Atmospheric Administration (grant no. NA23OAR4310300).

Acknowledgments

The authors thank Dr. Robert Wagner and Dr. Ottmar Möhler for valuable discussions on data comparison; Dr. Ana A. Piedehierro for providing data; William E. Schenk for laboratory support; and Dr. Xiaoli Shen and Dr. Justin Jacquot for assistance with PALMS-NG. We also thank Erick Norwood of the Jonathan Amy Facility for Chemical Instrumentation for instrument improvements. In addition, we acknowledge ChatGPT (Open AI, https://chatgpt.com) was used to improve language clarity and grammar of this research article.

https://doi.org/10.5194/egusphere-2026-2458
Preprint. Discussion started: 30 April 2026

References

Abbatt, J. P. D., Benz, S., Cziczo, D. J., Kanji, Z., Lohmann, U., and Möhler, O.: Solid Ammonium Sulfate Aerosols as Ice Nuclei: A Pathway for Cirrus Cloud Formation, Science, 313, 1770–1773, https://doi.org/10.1126/science.1129726, 2006.

Albrecht, B. A.: Aerosols, Cloud Microphysics, and Fractional Cloudiness, Science, 245, 1227–1230, https://doi.org/10.1126/science.245.4923.1227, 1989.

Bertozzi, B., Wagner, R., Höhler, K., Saathoff, H., Möhler, O., and Leisner, T.: Influence of the neutralization degree on the ice nucleation ability of ammoniated sulfate particles, J. Geophys. Res. Atmospheres, 129, e2023JD040078, https://doi.org/10.1029/2023JD040078, 2024.

Boucher, O., Randall, D., Artaxo, P., Bretherton, C., Feingold, G., Forster, P., Kerminen, V.-M., Kondo, Y., Liao, H., Lohmann, U., Rasch, P., Satheesh, S. K., Sherwood, S., Stevens, B., and Zhang, X. Y.: Clouds and aerosols, in: Climate Change 2013: The Physical Science Basis. Contribution of Working Group I to the Fifth Assessment Report of the Intergovernmental Panel on Climate Change, edited by: Stocker, T. F., Qin, D., Plattner, G.-K., Tignor, M., Allen, S. K., Doschung, J., Nauels, A., Xia, Y., Bex, V., and Midgley, P. M., Cambridge University Press, Cambridge, United Kingdom and New York, NY, USA, 571–657, https://doi.org/10.1017/CBO9781107415324.016, 2013.

Brüggemann, M., Xu, R., Tilgner, A., Kwong, K. C., Mutzel, A., Poon, H. Y., Otto, T., Schaefer, T., Poulain, L., Chan, M. N., and Herrmann, H.: Organosulfates in ambient aerosol: state of knowledge and future research directions on formation, abundance, fate, and importance, Environ. Sci. Technol., 54, 3767–3782, https://doi.org/10.1021/acs.est.9b06751, 2020.

Charnawskas, J. C., Alpert, P. A., Lambe, A. T., Berkemeier, T., O'Brien, R. E., Massoli, P., Onasch, T. B., Shiraiwa, M., Moffet, R. C., Gilles, M. K., Davidovits, P., Worsnop, D. R., and Knopf, D. A.: Condensed-phase biogenic–anthropogenic interactions with implications for cold cloud formation, Faraday Discuss., 200, 165–194, https://doi.org/10.1039/C7FD00010C, 2017.

Cooke, M. E., Armstrong, N. C., Fankhauser, A. M., Chen, Y., Lei, Z., Zhang, Y., Ledsky, I. R., Turpin, B. J., Zhang, Z., Gold, A., McNeill, V. F., Surratt, J. D., and Ault, A. P.: Decreases in epoxide-driven secondary organic aerosol production under highly acidic conditions: the importance of acid–base equilibria, Environ. Sci. Technol., 58, 10675–10684, https://doi.org/10.1021/acs.est.3c10851, 2024.

Cziczo, D. J. and Abbatt, J. P. D.: Ice nucleation in NH_4HSO_4, NH_4NO_3, and H_2SO_4 aqueous particles: Implications for cirrus cloud formation, Geophys. Res. Lett., 28, 963–966, https://doi.org/10.1029/2000GL012568, 2001.

Cziczo, D. J. and Froyd, K. D.: Sampling the composition of cirrus ice residuals, Atmospheric Res., 142, 15–31, https://doi.org/10.1016/j.atmosres.2013.06.012, 2014.

Cziczo, D. J., Nowak, J. B., Hu, J. H., and Abbatt, J. P. D.: Infrared spectroscopy of model tropospheric aerosols as a function of relative humidity: observation of deliquescence and crystallization, J. Geophys. Res. Atmospheres, 102, 18843–18850, https://doi.org/10.1029/97JD01361, 1997.

Cziczo, D. J., Froyd, K. D., Gallavardin, S. J., Moehler, O., Benz, S., Saathoff, H., and Murphy, D. M.: Deactivation of ice nuclei due to atmospherically relevant surface coatings, Environ. Res. Lett., 4, 044013, https://doi.org/10.1088/1748-9326/4/4/044013, 2009.

Cziczo, D. J., Froyd, K. D., Hoose, C., Jensen, E. J., Diao, M., Zondlo, M. A., Smith, J. B., Twohy, C. H., and Murphy, D. M.: Clarifying the Dominant Sources and Mechanisms of Cirrus Cloud Formation, Science, 340, 1320–1324, https://doi.org/10.1126/science.1234145, 2013.

https://doi.org/10.5194/egusphere-2026-2458
Preprint. Discussion started: 30 April 2026

Cziczo, D. J., Ladino, L., Boose, Y., Kanji, Z. A., Kupiszewski, P., Lance, S., Mertes, S., and Wex, H.: Measurements of Ice Nucleating Particles and Ice Residuals, Meteorol. Monogr., 58, 8.1-8.13, https://doi.org/10.1175/AMSMONOGRAPHS-D-16-0008.1, 2017.

DeCarlo, P. F., Kimmel, J. R., Trimborn, A., Northway, M. J., Jayne, J. T., Aiken, A. C., Gonin, M., Fuhrer, K., Horvath, T., Docherty, K. S., Worsnop, D. R., and Jimenez, J. L.: Field-deployable, high-resolution, time-of-flight aerosol mass spectrometer, Anal. Chem., 78, 8281–8289, https://doi.org/10.1021/ac061249n, 2006.

DeMott, P. J., Prenni, A. J., McMeeking, G. R., Sullivan, R. C., Petters, M. D., Tobo, Y., Niemand, M., Möhler, O., Snider, J. R., Wang, Z., and Kreidenweis, S. M.: Integrating laboratory and field data to quantify the immersion freezing ice nucleation activity of mineral dust particles, Atmospheric Chem. Phys., 15, 393–409, https://doi.org/10.5194/acp-15-393-2015, 2015.

DeRieux, W.-S. W., Li, Y., Lin, P., Laskin, J., Laskin, A., Bertram, A. K., Nizkorodov, S. A., and Shiraiwa, M.: Predicting the glass transition temperature and viscosity of secondary organic material using molecular composition, Atmospheric Chem. Phys., 18, 6331–6351, https://doi.org/10.5194/acp-18-6331-2018, 2018.

Finessi, E., Decesari, S., Paglione, M., Giulianelli, L., Carbone, C., Gilardoni, S., Fuzzi, S., Saarikoski, S., Raatikainen, T., Hillamo, R., Allan, J., Mentel, T. F., Tiitta, P., Laaksonen, A., Petäjä, T., Kulmala, M., Worsnop, D. R., and Facchini, M. C.: Determination of the biogenic secondary organic aerosol fraction in the boreal forest by NMR spectroscopy, Atmospheric Chem. Phys., 12, 941–959, https://doi.org/10.5194/acp-12-941-2012, 2012.

Forster, P., Storelvmo, T., Armour, K., Collins, W., Dufresne, J.-L., Frame, D., Lunt, D. J., Mauritsen, T., Palmer, M. D., Watanabe, M., Wild, M., and Zhang, H.: The Earth's energy budget, climate feedbacks, and climate sensitivity, in: Climate Change 2021: The Physical Science Basis. Contribution of Working Group I to the Sixth Assessment Report of the Intergovernmental Panel on Climate Change, edited by: Masson-Delmotte, V., Zhai, P., Pirani, A., Connors, S. L., Péan, C., Berger, S., Caud, N., Chen, Y., Goldfarb, L., Gomis, M. I., Huang, M., Leitzell, K., Lonnoy, E., Matthews, J. B. R., Maycock, T. K., Waterfield, T., Yelekçi, O., Yu, R., and Zhou, B., Cambridge University Press, Cambridge, United Kingdom and New York, NY, USA, 923–1054, https://doi.org/10.1017/9781009157896.009, 2021.

Froyd, K. D., Murphy, D. M., Lawson, P., Baumgardner, D., and Herman, R. L.: Aerosols that form subvisible cirrus at the tropical tropopause, Atmospheric Chem. Phys., 10, 209–218, https://doi.org/10.5194/acp-10-209-2010, 2010.

Garimella, S., Kristensen, T. B., Ignatius, K., Welti, A., Voigtländer, J., Kulkarni, G. R., Sagan, F., Kok, G. L., Dorsey, J., Nichman, L., Rothenberg, D. A., Rösch, M., Kirchgäßner, A. C. R., Ladkin, R., Wex, H., Wilson, T. W., Ladino, L. A., Abbatt, J. P. D., Stetzer, O., Lohmann, U., Stratmann, F., and Cziczo, D. J.: The SPectrometer for Ice Nuclei (SPIN): an instrument to investigate ice nucleation, Atmospheric Meas. Tech., 9, 2781–2795, https://doi.org/10.5194/amt-9-2781-2016, 2016.

Garimella, S., Rothenberg, D. A., Wolf, M. J., David, R. O., Kanji, Z. A., Wang, C., Rösch, M., and Cziczo, D. J.: Uncertainty in counting ice nucleating particles with continuous flow diffusion chambers, Atmospheric Chem. Phys., 17, 10855–10864, https://doi.org/10.5194/acp-17-10855-2017, 2017.

Glasius, M., Bering, M. S., Yee, L. D., De Sá, S. S., Isaacman-VanWertz, G., Wernis, R. A., Barbosa, H. M. J., Alexander, M. L., Palm, B. B., Hu, W., Campuzano-Jost, P., Day, D. A., Jimenez, J. L., Shrivastava, M., Martin, S. T., and Goldstein, A. H.: Organosulfates in aerosols downwind of an urban region in central amazon, Environ. Sci. Process. Impacts, 20, 1546–1558, https://doi.org/10.1039/C8EM00413G, 2018.

Grayson, J. W., Zhang, Y., Mutzel, A., Renbaum-Wolff, L., Böge, O., Kamal, S., Herrmann, H., Martin, S. T., and Bertram, A. K.: Effect of varying experimental conditions on the viscosity of α -pinene derived secondary organic material, Atmospheric Chem. Phys., 16, 6027–6040, https://doi.org/10.5194/acp-16-6027-2016, 2016.

https://doi.org/10.5194/egusphere-2026-2458
Preprint. Discussion started: 30 April 2026

Grayson, J. W., Evoy, E., Song, M., Chu, Y., Maclean, A., Nguyen, A., Upshur, M. A., Ebrahimi, M., Chan, C. K., Geiger, F. M., Thomson, R. J., and Bertram, A. K.: The effect of hydroxyl functional groups and molar mass on the viscosity of non-crystalline organic and organic–water particles, Atmospheric Chem. Phys., 17, 8509–8524, https://doi.org/10.5194/acp-17-8509-2017, 2017.

Guenther, A. B., Jiang, X., Heald, C. L., Sakulyanontvittaya, T., Duhl, T., Emmons, L. K., and Wang, X.: The model of emissions of gases and aerosols from nature version 2.1 (MEGAN2.1): an extended and updated framework for modeling biogenic emissions, Geosci. Model Dev., 5, 1471–1492, https://doi.org/10.5194/gmd-5-1471-2012, 2012.

Hallquist, M., Wenger, J. C., Baltensperger, U., Rudich, Y., Simpson, D., Claeys, M., Dommen, J., Donahue, N. M., George, C., Goldstein, A. H., Hamilton, J. F., Herrmann, H., Hoffmann, T., Iinuma, Y., Jang, M., Jenkin, M. E., Jimenez, J. L., Kiendler-Scharr, A., Maenhaut, W., McFiggans, G., Mentel, Th. F., Monod, A., Prévôt, A. S. H., Seinfeld, J. H., Surratt, J. D., Szmigielski, R., and Wildt, J.: The formation, properties and impact of secondary organic aerosol: current and emerging issues, Atmospheric Chem. Phys., 9, 5155–5236, https://doi.org/10.5194/acp-9-5155-2009, 2009.

Hendricks, J., Kärcher, B., and Lohmann, U.: Effects of ice nuclei on cirrus clouds in a global climate model, J. Geophys. Res., 116, D18206, https://doi.org/10.1029/2010JD015302, 2011.

Hettiyadura, A. P. S., Al-Naiema, I. M., Hughes, D. D., Fang, T., and Stone, E. A.: Organosulfates in Atlanta, Georgia: anthropogenic influences on biogenic secondary organic aerosol formation, Atmospheric Chem. Phys., 19, 3191–3206, https://doi.org/10.5194/acp-19-3191-2019, 2019.

Heymsfield, A. J., Krämer, M., Luebke, A., Brown, P., Cziczo, D. J., Franklin, C., Lawson, P., Lohmann, U., McFarquhar, G., Ulanowski, Z., and Van Tricht, K.: Cirrus Clouds, Meteorol. Monogr., 58, 2.1-2.26, https://doi.org/10.1175/AMSMONOGRAPHS-D-16-0010.1, 2017.

Hoose, C. and Möhler, O.: Heterogeneous ice nucleation on atmospheric aerosols: a review of results from laboratory experiments, Atmospheric Chem. Phys., 12, 9817–9854, https://doi.org/10.5194/acp-12-9817-2012, 2012.

Ignatius, K., Kristensen, T. B., Järvinen, E., Nichman, L., Fuchs, C., Gordon, H., Herenz, P., Hoyle, C. R., Duplissy, J., Garimella, S., Dias, A., Frege, C., Höppel, N., Tröstl, J., Wagner, R., Yan, C., Amorim, A., Baltensperger, U., Curtius, J., Donahue, N. M., Gallagher, M. W., Kirkby, J., Kulmala, M., Möhler, O., Saathoff, H., Schnaiter, M., Tomé, A., Virtanen, A., Worsnop, D., and Stratmann, F.: Heterogeneous ice nucleation of viscous secondary organic aerosol produced from ozonolysis of α -pinene, Atmospheric Chem. Phys., 16, 6495–6509, https://doi.org/10.5194/acp-16-6495-2016, 2016.

Iinuma, Y., Müller, C., Berndt, T., Böge, O., Claeys, M., and Herrmann, H.: Evidence for the Existence of Organosulfates from β-Pinene Ozonolysis in Ambient Secondary Organic Aerosol, Environ. Sci. Technol., 41, 6678–6683, https://doi.org/10.1021/es070938t, 2007a.

Iinuma, Y., Müller, C., Böge, O., Gnauk, T., and Herrmann, H.: The formation of organic sulfate esters in the limonene ozonolysis secondary organic aerosol (SOA) under acidic conditions, Atmos. Environ., 41, 5571–5583, https://doi.org/10.1016/j.atmosenv.2007.03.007, 2007b.

Jacquot, J. L., Shen, X., Abou-Ghanem, M., Froyd, K. D., Lawler, M., Schill, G. P., Slovacek, K., Thomson, D. S., Cziczo, D. J., and Murphy, D. M.: A new airborne single particle mass spectrometer: PALMS-NG, Aerosol Sci. Technol., 58, 991–1007, https://doi.org/10.1080/02786826.2024.2331549, 2024.

Kärcher, B., DeMott, P. J., Jensen, E. J., and Harrington, J. Y.: Studies on the competition between homogeneous and heterogeneous ice nucleation in cirrus formation, J. Geophys. Res. Atmospheres, 127, e2021JD035805, https://doi.org/10.1029/2021JD035805, 2022.

https://doi.org/10.5194/egusphere-2026-2458
Preprint. Discussion started: 30 April 2026

Kasparoglu, S., Perkins, R., Ziemann, P. J., DeMott, P. J., Kreidenweis, S. M., Finewax, Z., Deming, B. L., DeVault, M. P., and Petters, M. D.: Experimental Determination of the Relationship Between Organic Aerosol Viscosity and Ice Nucleation at Upper Free Tropospheric Conditions, J. Geophys. Res. Atmospheres, 127, e2021JD036296, https://doi.org/10.1029/2021JD036296, 2022.

Knopf, D. A., Alpert, P. A., and Wang, B.: The Role of Organic Aerosol in Atmospheric Ice Nucleation: A Review, ACS Earth Space Chem., 2, 168–202, https://doi.org/10.1021/acsearthspacechem.7b00120, 2018.

Koehler, K. A., Kreidenweis, S. M., DeMott, P. J., Petters, M. D., Prenni, A. J., and Möhler, O.: Laboratory investigations of the impact of mineral dust aerosol on cold cloud formation, Atmospheric Chem. Phys., 10, 11955–11968, https://doi.org/10.5194/acp-10-11955-2010, 2010.

Koop, T.: Homogeneous Ice Nucleation in Water and Aqueous Solutions, Z. Für Phys. Chem., 218, 1231–1258, https://doi.org/10.1524/zpch.218.11.1231.50812, 2004.

Koop, T., Luo, B., Tsias, A., and Peter, T.: Water activity as the determinant for homogeneous ice nucleation in aqueous solutions, Nature, 406, 611–614, https://doi.org/10.1038/35020537, 2000.

Koop, T., Bookhold, J., Shiraiwa, M., and Pöschl, U.: Glass transition and phase state of organic compounds: dependency on molecular properties and implications for secondary organic aerosols in the atmosphere, Phys. Chem. Chem. Phys., 13, 19238, https://doi.org/10.1039/c1cp22617g, 2011.

Kulkarni, G., China, S., Liu, S., Nandasiri, M., Sharma, N., Wilson, J., Aiken, A. C., Chand, D., Laskin, A., Mazzoleni, C., Pekour, M., Shilling, J., Shutthanandan, V., Zelenyuk, A., and Zaveri, R. A.: Ice nucleation activity of diesel soot particles at cirrus relevant temperature conditions: Effects of hydration, secondary organics coating, soot morphology, and coagulation, Geophys. Res. Lett., 43, 3580–3588, https://doi.org/10.1002/2016GL068707, 2016.

Ladino, L. A., Zhou, S., Yakobi-Hancock, J. D., Aljawhary, D., and Abbatt, J. P. D.: Factors controlling the ice nucleating abilities of α -pinene SOA particles, J. Geophys. Res. Atmospheres, 119, 9041–9051, https://doi.org/10.1002/2014JD021578, 2014.

Lambe, A. T., Ahern, A. T., Williams, L. R., Slowik, J. G., Wong, J. P. S., Abbatt, J. P. D., Brune, W. H., Ng, N. L., Wright, J. P., Croasdale, D. R., Worsnop, D. R., Davidovits, P., and Onasch, T. B.: Characterization of aerosol photooxidation flow reactors: heterogeneous oxidation, secondary organic aerosol formation and cloud condensation nuclei activity measurements, Atmospheric Meas. Tech., 4, 445–461, https://doi.org/10.5194/amt-4-445-2011, 2011a.

Lambe, A. T., Onasch, T. B., Massoli, P., Croasdale, D. R., Wright, J. P., Ahern, A. T., Williams, L. R., Worsnop, D. R., Brune, W. H., and Davidovits, P.: Laboratory studies of the chemical composition and cloud condensation nuclei (CCN) activity of secondary organic aerosol (SOA) and oxidized primary organic aerosol (OPOA), Atmospheric Chem. Phys., 11, 8913–8928, https://doi.org/10.5194/acp-11-8913-2011, 2011b.

Lei, Z., Chen, Y., Zhang, Y., Cooke, M. E., Ledsky, I. R., Armstrong, N. C., Olson, N. E., Zhang, Z., Gold, A., Surratt, J. D., and Ault, A. P.: Initial pH Governs Secondary Organic Aerosol Phase State and Morphology after Uptake of Isoprene Epoxydiols (IEPOX), Environ. Sci. Technol., 56, 10596–10607, https://doi.org/10.1021/acs.est.2c01579, 2022.

Li, X., Wolf, M., Shen, X., Steinke, I., Lai, Z., Niu, S., China, S., Shrivastava, M., Zhang, Z., Gold, A., Surratt, J. D., Bourg, I. C., Cziczo, D. J., Burrows, S. M., and Zhang, Y.: Quantifying and Modeling the Impact of Phase State on the Ice Nucleation Abilities of 2-Methyltetrols as a Key Component of Secondary Organic Aerosol Derived from Isoprene Epoxydiols, Environ. Sci. Technol., 58, 22678–22690, https://doi.org/10.1021/acs.est.4c06285, 2024.

https://doi.org/10.5194/egusphere-2026-2458
Preprint. Discussion started: 30 April 2026

Li, Y., Day, D. A., Stark, H., Jimenez, J. L., and Shiraiwa, M.: Predictions of the glass transition temperature and viscosity of organic aerosols from volatility distributions, Atmospheric Chem. Phys., 20, 8103–8122, https://doi.org/10.5194/acp-20-8103-2020, 2020.

Lohmann, U., Spichtinger, P., Jess, S., Peter, T., and Smit, H.: Cirrus cloud formation and ice supersaturated regions in a global climate model, Environ. Res. Lett., 3, 45022, https://doi.org/10.1088/1748-9326/3/4/045022, 2008.

Mahrt, F., Nikkho, S., Zaks, J., Uppal, G., Lam, A., Ammann, M., and Bertram, A. K.: Surprising crystallinity of biomass burning secondary organic aerosol from catechol and nitrate radical reactions: evidence and possible implications, Environ. Sci. Technol., 59, 16923–16932, https://doi.org/10.1021/acs.est.5c06834, 2025.

Marcolli, C.: Deposition nucleation viewed as homogeneous or immersion freezing in pores and cavities, Atmospheric Chem. Phys., 14, 2071–2104, https://doi.org/10.5194/acp-14-2071-2014, 2014.

Möhler, O., Benz, S., Saathoff, H., Schnaiter, M., Wagner, R., Schneider, J., Walter, S., Ebert, V., and Wagner, S.: The effect of organic coating on the heterogeneous ice nucleation efficiency of mineral dust aerosols, Environ. Res. Lett., 3, 025007, https://doi.org/10.1088/1748-9326/3/2/025007, 2008.

Murphy, D. M.: The design of single particle laser mass spectrometers, Mass Spectrom. Rev., 26, 150–165, https://doi.org/10.1002/mas.20113, 2007.

Murray, B. J., Wilson, T. W., Dobbie, S., Cui, Z., Al-Jumur, S. M. R. K., Möhler, O., Schnaiter, M., Wagner, R., Benz, S., Niemand, M., Saathoff, H., Ebert, V., Wagner, S., and Kärcher, B.: Heterogeneous nucleation of ice particles on glassy aerosols under cirrus conditions, Nat. Geosci., 3, 233–237, https://doi.org/10.1038/ngeo817, 2010.

Nikkho, S., Bai, B., Mahrt, F., Zaks, J., Peng, L., Kiland, K. J., Liu, P., and Bertram, A. K.: Secondary Organic Aerosol from Biomass Burning Phenolic Compounds and Nitrate Radicals can be Highly Viscous over a Wide Relative Humidity Range, Environ. Sci. Technol., 58, 21702–21715, https://doi.org/10.1021/acs.est.4c06235, 2024.

Niu, S., McCary, K. P., Alton, M., Krechmer, J. E., Stark, H., Surratt, J. D., Canagaratna, M., and Zhang, Y.: Simultaneously characterizing the volatility distribution and phase state of submicron secondary organic aerosols using a vocus vaporization inlet for aerosols with a chemical ionization mass spectrometer, ACS EST Air, acsestair.5c00155, https://doi.org/10.1021/acsestair.5c00155, 2025.

Nozière, B., Kalberer, M., Claeys, M., Allan, J., D'Anna, B., Decesari, S., Finessi, E., Glasius, M., Grgić, I., Hamilton, J. F., Hoffmann, T., Iinuma, Y., Jaoui, M., Kahnt, A., Kampf, C. J., Kourtchev, I., Maenhaut, W., Marsden, N., Saarikoski, S., Schnelle-Kreis, J., Surratt, J. D., Szidat, S., Szmigielski, R., and Wisthaler, A.: The molecular identification of organic compounds in the atmosphere: state of the art and challenges, Chem. Rev., 115, 3919–3983, https://doi.org/10.1021/cr5003485, 2015.

Piedehierro, A. A., Welti, A., Buchholz, A., Korhonen, K., Pullinen, I., Summanen, I., Virtanen, A., and Laaksonen, A.: Ice nucleation on surrogates of boreal forest SOA particles: effect of water content and oxidative age, Atmospheric Chem. Phys., 21, 11069–11078, https://doi.org/10.5194/acp-21-11069-2021, 2021.

Pruppacher, H. R. and Klett, J. D.: Microphysics of clouds and precipitation, Springer Netherlands, Dordrecht, https://doi.org/10.1007/978-0-306-48100-0, 2010.

Pye, H. O. T., Chan, A. W. H., Barkley, M. P., and Seinfeld, J. H.: Global modeling of organic aerosol: the importance of reactive nitrogen (NO_x and NO_3), Atmospheric Chem. Phys., 10, 11261–11276, https://doi.org/10.5194/acp-10-11261-2010, 2010.

https://doi.org/10.5194/egusphere-2026-2458
Preprint. Discussion started: 30 April 2026

Raatikainen, T., Vaattovaara, P., Tiitta, P., Miettinen, P., Rautiainen, J., Ehn, M., Kulmala, M., Laaksonen, A., and Worsnop, D. R.: Physicochemical properties and origin of organic groups detected in boreal forest using an aerosol mass spectrometer, Atmospheric Chem. Phys., 10, 2063–2077, https://doi.org/10.5194/acp-10-2063-2010, 2010.

Rapp, C. N., Carrillo-Cardenas, G., Niu, S., Zhang, Y., Brechtel, F. J., Hallar, A. G., and Cziczo, D. J.: Curve fitting algorithm for multimodal particle size distributions – a theoretical basis, https://doi.org/10.5194/egusphere-2025-4222, 19 December 2025a.

Rapp, C. N., Niu, S., Armstrong, N. C., Shen, X., Berkemeier, T., Surratt, J. D., Zhang, Y., and Cziczo, D. J.: Ice-nucleating properties of glassy organic and organosulfate aerosol, Atmospheric Chem. Phys., 25, 5519–5536, https://doi.org/10.5194/acp-25-5519-2025, 2025b.

Renbaum-Wolff, L., Grayson, J. W., Bateman, A. P., Kuwata, M., Sellier, M., Murray, B. J., Shilling, J. E., Martin, S. T., and Bertram, A. K.: Viscosity of α -pinene secondary organic material and implications for particle growth and reactivity, Proc. Natl. Acad. Sci., 110, 8014–8019, https://doi.org/10.1073/pnas.1219548110, 2013.

Rothfuss, N. E. and Petters, M. D.: Coalescence-based assessment of aerosol phase state using dimers prepared through a dual-differential mobility analyzer technique, Aerosol Sci. Technol., 50, 1294–1305, https://doi.org/10.1080/02786826.2016.1221050, 2016.

Schill, G. P. and Tolbert, M. A.: Depositional Ice Nucleation on Monocarboxylic Acids: Effect of the O:C Ratio, J. Phys. Chem. A, 116, 6817–6822, https://doi.org/10.1021/jp301772q, 2012.

Schill, G. P. and Tolbert, M. A.: Heterogeneous ice nucleation on phase-separated organic-sulfate particles: effect of liquid vs. glassy coatings, Atmospheric Chem. Phys., 13, 4681–4695, https://doi.org/10.5194/acp-13-4681-2013, 2013.

Shiraiwa, M., Li, Y., Tsimpidi, A. P., Karydis, V. A., Berkemeier, T., Pandis, S. N., Lelieveld, J., Koop, T., and Pöschl, U.: Global distribution of particle phase state in atmospheric secondary organic aerosols, Nat. Commun., 8, 15002, https://doi.org/10.1038/ncomms15002, 2017.

Shrivastava, M., Cappa, C. D., Fan, J., Goldstein, A. H., Guenther, A. B., Jimenez, J. L., Kuang, C., Laskin, A., Martin, S. T., Ng, N. L., Petaja, T., Pierce, J. R., Rasch, P. J., Roldin, P., Seinfeld, J. H., Shilling, J., Smith, J. N., Thornton, J. A., Volkamer, R., Wang, J., Worsnop, D. R., Zaveri, R. A., Zelenyuk, A., and Zhang, Q.: Recent advances in understanding secondary organic aerosol: implications for global climate forcing, Rev. Geophys., 55, 509–559, https://doi.org/10.1002/2016RG000540, 2017.

Staudt, S., Kundu, S., Lehmler, H.-J., He, X., Cui, T., Lin, Y.-H., Kristensen, K., Glasius, M., Zhang, X., Weber, R. J., Surratt, J. D., and Stone, E. A.: Aromatic organosulfates in atmospheric aerosols: synthesis, characterization, and abundance, Atmos. Environ., 94, 366–373, https://doi.org/10.1016/j.atmosenv.2014.05.049, 2014.

Surratt, J. D., Kroll, J. H., Kleindienst, T. E., Edney, E. O., Claeys, M., Sorooshian, A., Ng, N. L., Offenberg, J. H., Lewandowski, M., Jaoui, M., Flagan, R. C., and Seinfeld, J. H.: Evidence for organosulfates in secondary organic aerosol, Environ. Sci. Technol., 41, 517–527, https://doi.org/10.1021/es062081q, 2007.

Surratt, J. D., Gómez-González, Y., Chan, A. W. H., Vermeylen, R., Shahgholi, M., Kleindienst, T. E., Edney, E. O., Offenberg, J. H., Lewandowski, M., Jaoui, M., Maenhaut, W., Claeys, M., Flagan, R. C., and Seinfeld, J. H.: Organosulfate Formation in Biogenic Secondary Organic Aerosol, J. Phys. Chem. A, 112, 8345–8378, https://doi.org/10.1021/jp802310p, 2008.

Thomas, L. H., Meatyard, R., Smith, H., and Davies, G. H.: Viscosity behavior of associated liquids at lower temperatures and vapor pressures, J. Chem. Eng. Data, 24, 161–164, https://doi.org/10.1021/je60082a011, 1979.

https://doi.org/10.5194/egusphere-2026-2458
Preprint. Discussion started: 30 April 2026

Tolocka, M. P., Jang, M., Ginter, J. M., Cox, F. J., Kamens, R. M., and Johnston, M. V.: Formation of oligomers in secondary organic aerosol, Environ. Sci. Technol., 38, 1428–1434, https://doi.org/10.1021/es035030r, 2004.

Twomey, S. A., Piepgrass, M., and Wolfe, T. L.: An assessment of the impact of pollution on global cloud albedo, Tellus B, 36B, 356–366, https://doi.org/10.1111/j.1600-0889.1984.tb00254.x, 1984.

Vali, G.: Sizes of Atmospheric Ice Nuclei, Nature, 212, 384–385, https://doi.org/10.1038/212384a0, 1966.

Wagner, R., Höhler, K., Huang, W., Kiselev, A., Möhler, O., Mohr, C., Pajunoja, A., Saathoff, H., Schiebel, T., Shen, X., and Virtanen, A.: Heterogeneous ice nucleation of α -pinene SOA particles before and after ice cloud processing, J. Geophys. Res. Atmospheres, 122, 4924–4943, https://doi.org/10.1002/2016JD026401, 2017.

Wolf, M. J., Zhang, Y., Zawadowicz, M. A., Goodell, M., Froyd, K., Freney, E., Sellegri, K., Rösch, M., Cui, T., Winter, M., Lacher, L., Axisa, D., DeMott, P. J., Levin, E. J. T., Gute, E., Abbatt, J., Koss, A., Kroll, J. H., Surratt, J. D., and Cziczo, D. J.: A biogenic secondary organic aerosol source of cirrus ice nucleating particles, Nat. Commun., 11, 4834, https://doi.org/10.1038/s41467-020-18424-6, 2020.

Zelinka, M. D., Randall, D. A., Webb, M. J., and Klein, S. A.: Clearing clouds of uncertainty, Nat. Clim. Change, 7, 674–678, https://doi.org/10.1038/nclimate3402, 2017.

Zhang, H., Yee, L. D., Lee, B. H., Curtis, M. P., Worton, D. R., Isaacman-VanWertz, G., Offenberg, J. H., Lewandowski, M., Kleindienst, T. E., Beaver, M. R., Holder, A. L., Lonneman, W. A., Docherty, K. S., Jaoui, M., Pye, H. O. T., Hu, W., Day, D. A., Campuzano-Jost, P., Jimenez, J. L., Guo, H., Weber, R. J., de Gouw, J., Koss, A. R., Edgerton, E. S., Brune, W., Mohr, C., Lopez-Hilfiker, F. D., Lutz, A., Kreisberg, N. M., Spielman, S. R., Hering, S. V., Wilson, K. R., Thornton, J. A., and Goldstein, A. H.: Monoterpenes are the largest source of summertime organic aerosol in the southeastern United States, Proc. Natl. Acad. Sci. U. S. A., 115, 2038–2043, https://doi.org/10.1073/pnas.1717513115, 2018.

Zhang, Y., Sanchez, M. S., Douet, C., Wang, Y., Bateman, A. P., Gong, Z., Kuwata, M., Renbaum-Wolff, L., Sato, B. B., Liu, P. F., Bertram, A. K., Geiger, F. M., and Martin, S. T.: Changing shapes and implied viscosities of suspended submicron particles, Atmospheric Chem. Phys., 15, 7819–7829, https://doi.org/10.5194/acp-15-7819-2015, 2015.